Kernel Current Source Density Method

Article *in* Neural Computation · November 2011

DOI: 10.1162/NECO_a_00236 · Source: PubMed

4 authors, including:

Jan Potworowski
Nencki Institute of Experimental Biology
5 PUBLICATIONS **198** CITATIONS

SEE PROFILE

Wit Jakuczun
F33.ai
11 PUBLICATIONS **115** CITATIONS

SEE PROFILE

Daniel K Wojcik
Nencki Institute of Experimental Biology
142 PUBLICATIONS **1,781** CITATIONS

SEE PROFILE

Kernel Current Source Density Method

Jan Potworowski[1], Wit Jakuczun[2], Szymon Łęski[1], Daniel Wójcik[1]

[1] Department of Neurophysiology,
Nencki Institute of Experimental Biology,
3 Pasteur Street, 02-093 Warsaw, Poland

[2] WLOG Solutions, Warsaw, Poland

October 12, 2010

Abstract

Local field potentials (LFP), the low-frequency part of extracellular electrical recordings, are a measure of the neural activity reflecting dendritic processing of synaptic inputs to neuronal populations.

To localize synaptic dynamics it is convenient, whenever possible, to estimate the density of trans-membrane current sources (CSD) generating the LFP.

In this work we propose a new framework, kernel Current Source Density method (kCSD), for non-parametric estimation of CSD from LFP recorded from arbitrarily distributed electrodes using kernel methods. We test specific implementations of this framework on model data measured with one-, two-, and three-dimensional multi-electrode setups. We compare these methods with the traditional approach through numerical approximation of the Laplacian and with the recently developed inverse Current Source Density methods (iCSD). We show that iCSD is a special case of kCSD. The proposed method opens up new experimental possibilites of CSD analysis from already taken or new recordings on arbitrarily distributed electrodes (not necessarily on a grid), which can be obtained in extracellular recordings of single unit activity with multiple electrodes.

1 Introduction

Extracellular recordings of electric potential have great significance in the studies of neural activity in vivo. In the last few years we have witnessed rapid development of technology for large scale electrical recordings. Various types of multielectrodes were devised to simultaneously record extracellular potentials from multiple spatial locations (Normann et al. 1999, Csicsvari et al. 2003, Barthó et al. 2004, Buzsáki 2004, Sher et al. 2007, Imfeld et al. 2008, Frey et al. 2009, Ward et al. 2009, Charvet et al. 2010). The low-frequency part of these recordings, the local field potentials (LFP), typically reflect the dendritic processing of synaptic inputs (Nunez & Srinivasan 2005, Einevoll et al. 2007, Pettersen et al. 2008, Lindén et al. 2010). Direct interpretation of LFP is difficult as it is a nonlocal

measure of the neural activity: it may have contributions from neurons located more than a millimeter away from the electrode (Kreiman et al. 2006, Liu & Newsome 2006, Berens et al. 2008, Katzner et al. 2009, Xing et al. 2009) or even a few milimeters (Hunt et al. 2010). Therefore, if only possible it is convenient to estimate the current source density (CSD), the volume density of net transmembrane currents, generating the LFP (Lorente de No 1947, Pitts 1952, Plonsey 1969, Freeman & Nicholson 1975, Nicholson & Freeman 1975, Mitzdorf 1985). CSD directly relates to the local neural activity and current source density analysis is a convenient tool for analysis of LFP recorded from multielectrodes (Haberly & Shepherd 1973, Mitzdorf 1985, Schroeder et al. 1992, Ylinen et al. 1995, Lakatos et al. 2005, Lipton et al. 2006, Rajkai et al. 2008, de Solages et al. 2008).

Since CSD in a homogeneous and isotropic tissue is given by the Laplacian of the potentials, originally it was estimated by a discrete differentiation scheme from the potentials measured on a regular grid (Freeman & Nicholson 1975, Nicholson & Freeman 1975, Mitzdorf 1985). In the past few years a new method for CSD estimation has been developed, the inverse CSD (iCSD) method (Pettersen et al. 2006, Łęski, Wójcik, Tereszczuk, Świejkowski, Kublik & Wróbel 2007, Wójcik & Łęski 2010, Łęski, Pettersen, Tunstall, Einevoll, Gigg & Wójcik 2010). The main idea behind iCSD is to assume a specific parametric form of CSD generating the measured potentials (e.g. spline interpolated between the grid nodes), calculate the LFP in a forward-modeling scheme to obtain the values of CSD parameters (e.g. CSD values at the nodes) by matching the experimental data with computed values. The iCSD framework requires an assumption of a specific geometry of contacts requiring new calculations for each distribution of electrodes. So far, all the propositions assumed recordings on regular, Cartesian grids.

Here we introduce a new, non-parametric method for CSD estimation. The kernel CSD method (kCSD) is based on kernel methods, widely used in machine learning (Vapnik 1998, Schoelkopf & Smola 2002, Shawe-Taylor & Christiani 2004). This method does not require the user to specify the restricted, parametrized form of the admissible CSD distributions. Instead, one specifies an arbitrarily broad family of possible distributions and uniqueness of the solution is guaranteed by the minimum-norm requirement built in the method.

The assumption of regular electrode arrangement is not necessary, kCSD can be applied to recordings from electrodes distributed at any positions on one-, two-, and three-dimensional sets with equal ease. Moreover, we show that kCSD is a general non-parametric framework for CSD estimation including all the previous variants of iCSD methods as special cases.

The article is organized as follows: in Section 2 we introduce the basic framework of reproducing kernels. We define reproducing kernel Hilbert spaces (RKHS) (Aronszajn 1950, Vapnik 1998, Schoelkopf & Smola 2002, Shawe-Taylor & Christiani 2004) and show possible ways of constructing them. We also demonstrate an efficient regression algorithm applicable in RKHS. However, our task of estimating CSD from measured potentials is a more complicated problem than a regular regression task: the fact that the CSD and the potentials are different physical quantities forces us to solve a linear operator equation.

In Section 3 we show how to use the regression algorithm introduced in Section 2 to obtain a scheme for solving linear operator equations, provided that the image of the linear operator has a structure of RKHS (Vapnik 1998). Next we apply this technique to estimate the most plausible CSD consistent with the measured potentials. We show how to do this in cases where the measurements were taken on sets of different dimensionality, e.g. for laminar multielectrodes, multi-shaft multielectrodes, and in the general three-dimensional case. We also show here that the previously introduced iCSD methods are special cases

of kCSD introduced here.

To test the viability of the proposed scheme we performed a number of tests on model data where we control the sources to be recovered from potentials. These tests are presented in Section 4. We first consider the case of regular grids, as these are the only cases that were treated by the methods available so far, to show how the new method compares with the readily available alternatives. Then we consider the case of arbitrary distributions of contacts as the proposed methods can easily treat arbitrary geometry of the electrode setup. The properties of the proposed method, further directions of development, and the significance of the kernel approach are discussed in the final section.

2 Reproducing Kernels

2.1 Introduction to Reproducing Kernels

We start with defining a reproducing kernel Hilbert space. Let's introduce a mapping $\phi : \mathbb{R}^d \to \mathbb{R}^n$. It is important to stress that n can be very large. This means that the function ϕ transforms d-dimensional feature vectors into a possibly very large number of new features. The idea of the transformation is to encode the CSD problem by handcrafted mappings. All definitions in this section are based on Shawe-Taylor & Christiani (2004), Chapter 3.2.

Definition 2.1 *A kernel function (a kernel for short) $K : \mathbb{R}^d \times \mathbb{R}^d \longrightarrow \mathbb{R}$ is defined by the following equation*

$$K(x, x') = \langle \phi(x), \phi(x') \rangle \tag{1}$$

where $\langle \cdot, \cdot \rangle$ is the inner product in $\mathbb{R}^n$.

Having a *kernel function* we can introduce the *Reproducing Kernel Hilbert Space (RKHS)* generated by this kernel.

Definition 2.2 *The Reproducing Kernel Hilbert Space generated by a kernel function K is defined as follows*

$$\mathcal{H} = \left\{ \sum_{i=1}^{l} \alpha_i K(x_i, x) : l \in \mathbb{N}, x_i \in \mathbb{R}^d, \alpha_i \in \mathbb{R}, i = 1, ..., l \right\}. \tag{2}$$

The inner product in this space is given by the following formula

$$\langle f, g \rangle_{\mathcal{H}} = \sum_{i=1}^{l} \sum_{j=1}^{m} \alpha_i \beta_j K(x_i, z_j), \tag{3}$$

where $f(x) = \sum_{i=1}^{l} \alpha_i K(x_i, x)$ and $g(x) = \sum_{j=1}^{m} \beta_j K(z_j, x)$. The norm in $\mathcal{H}$ is given by:

$$\|f\|^2_{\mathcal{H}} = \langle f, f \rangle_{\mathcal{H}}.$$

The kernel has the following properties:

Reproducibility For $f = \sum_{i=1}^{l} \alpha_i K(x_i, x) \in \mathcal{H}$ the following equation holds

$$\langle f, K(x, \cdot) \rangle_{\mathcal{H}} = \sum_{i=1}^{l} \alpha_i K(x_i, x) = f(x).$$

Finite semi-definiteness For any number $l \in \mathbb{N}$ and any l vectors $x_1, ..., x_l$, where $x_i \in \mathbb{R}^d$, the matrix $\mathbf{K} = \{K(x_i, x_j)\}_{i,j=1,...,l}$ is semi definite. That is

$$\forall \mathbf{v} \in \mathbb{R}^l : \quad \mathbf{v}^T \mathbf{K} \mathbf{v} \geq 0. \tag{4}$$

Proofs of these facts and a thorough exposition of RKHS theory can be found in Shawe-Taylor & Christiani (2004), Chapter 3.2.

2.2 Kernel construction for a finite dimensional space

Let us now consider a finite set of linearly independent functions $b_1(x), ..., b_n(x) : \mathbb{R}^d \longrightarrow \mathbb{R}$ and a linear space of functions spanned by this set:

$$\mathcal{F} = \{f(x) = a_1 b_1(x) + ... + a_n b_n(x) : a_1, ..., a_n \in \mathbb{R}\}. \tag{5}$$

We introduce a norm in $\mathcal{F}$:

$$\|f\|_{\mathcal{F}} = \sqrt{\sum_{i=1}^{n} a_i^2}$$

and define a kernel $K : \mathbb{R}^d \times \mathbb{R}^d \longrightarrow \mathbb{R}$ by

$$K(x, y) = \sum_{i=1}^{n} b_i(x) b_i(y). \tag{6}$$

It is easy to see that K is a kernel function according to Definition 2.1. It is sufficient to define ϕ stated in Definition 2.1 as:

$$\phi : \mathbb{R}^d \longrightarrow \mathbb{R}^n; x \longmapsto \begin{bmatrix} b_1(x) \\ \vdots \\ b_n(x) \end{bmatrix}.$$

Let us introduce an RKHS by taking $\mathcal{H}$ according to Definition 2.2 with the kernel K defined in (6). Then the following theorem holds:

Theorem 2.3
(i) $f \in \mathcal{H} \Rightarrow f \in \mathcal{F}$, therefore, $\mathcal{H} \subset \mathcal{F}$
(ii) $f \in \mathcal{F} \Rightarrow \exists n \in \mathbb{N}, x_1, ..., x_n \in \mathbb{R}^n$, and $\alpha_1, ..., \alpha_n \in \mathbb{R} : f(x) = \sum_{i=1}^{n} \alpha_i K(x_i, x)$, therefore, $\mathcal{F} \subset \mathcal{H}$
(iii) $\|f\|_{\mathcal{F}} = \|f\|_{\mathcal{H}}$.

Theorem 2.3 shows that $\mathcal{F}$ and $\mathcal{H}$ contain the same elements and have equal norms, so they can be considered equivalent. The proof can be found in Appendix A.1.

2.3 Regression in RKHS spaces

We now introduce a theorem suggesting how to construct estimators of functions in a given RKHS $\mathcal{H}$ generated by a kernel function K. Suppose we observe k values of some function $f \in \mathcal{F}:\quad (x_i, f_i)_{i=1}^k$ where $x_i \in \mathbb{R}^n$, and $f_i \in \mathbb{R}$. Let's introduce a function err:

$$\text{err} : \mathcal{H} \longrightarrow \mathbb{R}; f \mapsto \sum_{i=1}^{k} (f(x_i) - f_i)^2, \tag{7}$$

which we call the *empirical risk*. Let $\mathcal{M}$ denote the set of functions in $\mathcal{H}$ that minimise err. We call $\mathcal{M}$ the set of *empirical risk minimizers*.

Theorem 2.4 *If matrix*

$$\begin{bmatrix} K(x_1, x_1) & \dots & K(x_1, x_k) \\ \vdots & \ddots & \vdots \\ K(x_k, x_1) & \dots & K(x_k, x_k) \end{bmatrix}$$

is invertible, there exist $\beta_1, ..., \beta_k \in \mathbb{R}$ *such that*

$$f^*(x) = \sum_{i=1}^{k} \beta_i K(x_i, x) \in \mathcal{M}. \tag{8}$$

Moreover:

$$f^* = \underset{f \in \mathcal{M}}{\text{argmin}} \|f\|_{\mathcal{H}} \tag{9}$$

and $\text{err}(f^*) = 0$.

The proof can be found in the Appendix A.2.

If $\mathcal{H}$ was constructed from a finite dimensional space $\mathcal{F}$ defined in (5) with the kernel function from (6), minimizing the norm in $\mathcal{H}$ implies minimizing $\sqrt{\sum a_i^2}$, the norm in $\mathcal{F}$, which can be interpreted as minimizing the energy of the solution or smoothing.

Theorems 2.3 and 2.4 give a powerful tool for estimation. Having a set of observations we are free to choose a hypothesis space $\mathcal{F}$ in which we want to carry out the estimation by defining its basis. We can do this according to our intuition on the structure of the data we observe. Several examples are shown in the next section. The dimension of space $\mathcal{F}$ can be very high, much higher than the number of observations. Theorem 2.3 shows how to find an RKHS $\mathcal{H}$ containing the same elements as $\mathcal{F}$. Using Theorem 2.4 we find the empirical risk minimizer in $\mathcal{H}$ (and thus in $\mathcal{F}$) with the smallest norm.

3 The Kernel Current Source Density (kCSD) Method

In his seminal book, Vapnik (1998) showed how RKHS theory can be applied to solving linear operator equations. We start this section with a brief review of this theory. Next we restrict ourselves to the specific case of estimating current source density from a set of recorded LFPs and show how it can can be formulated as a linear operator equation problem. We introduce a general scheme, which we call the kCSD method. In Section 3.3 we show that the previously developed iCSD methods (Pettersen et al. 2006, Łęski, Wójcik, Tereszczuk, Świejkowski, Kublik & Wróbel 2007, Łęski, Pettersen, Tunstall, Einevoll, Gigg & Wójcik 2010) are special cases of that scheme.

3.1 RKHS approach to solving linear operator equations

Consider a pair of n-dimensional function spaces: $\widetilde{\mathcal{F}}$ (the "source" space) and $\mathcal{F}$ (the "potentials" space). Each of these spaces is spanned by n basis functions:

$$\widetilde{\mathcal{F}} = \left\{ f(x) = a_1 \widetilde{b}_1(x) + ... + a_n \widetilde{b}_n(x) : \widetilde{b}_i : \mathbb{R}^d \longrightarrow \mathbb{R} \right\}, \tag{10}$$

$$\mathcal{F} = \left\{ f(x) = a_1 b_1(x) + ... + a_n b_n(x) \ : \ b_i : \mathbb{R}^d \longrightarrow \mathbb{R} \right\}. \tag{11}$$

Let $\mathcal{A} : \widetilde{\mathcal{F}} \longrightarrow \mathcal{F}$ be a linear operator such that $\mathcal{A}\widetilde{b}_i = b_i$. Motivated by Vapnik (1998), Chapter 11.9, we suggest how to estimate a function $\widetilde{f} \in \widetilde{\mathcal{F}}$ ("source") such that $\mathcal{A}\widetilde{f} = f$, given measurements of f : $(x_i, f_i)_{i=1}^k$ (the "potentials").

Take $\widetilde{f} \in \widetilde{\mathcal{F}}, f \in \mathcal{F}$ such that $\mathcal{A}\widetilde{f} = f$. We define the norms in $\mathcal{F}$ and $\widetilde{\mathcal{F}}$ by

$$\|f\|_{\mathcal{F}} = \|\widetilde{f}\|_{\widetilde{\mathcal{F}}} = \sqrt{\sum_{i=1}^{n} a_i^2}. \tag{12}$$

For our set of observations $(x_i, f_i)_{i=1}^k$ we introduce function $\mathrm{err}_{\mathcal{A}}$:

$$\mathrm{err}_{\mathcal{A}} : \widetilde{\mathcal{F}} \longrightarrow \mathbb{R}; \widetilde{f} \mapsto \sum_{i=1}^{k} (f(x_i) - f_i)^2, \quad \text{where} \quad \mathcal{A}\widetilde{f} = f.$$

Let $\mathcal{M}_{\mathcal{A}}$ denote the set of functions $\widetilde{f} \in \widetilde{\mathcal{F}}$ that minimize $\mathrm{err}_{\mathcal{A}}$. Solving the linear operator equation in general, consists of finding a solution in $\mathcal{M}_{\mathcal{A}}$, which is an ill-posed problem (Vapnik 1998). We will make the problem well-defined by looking for a specific solution $\widetilde{f}^* \in \mathcal{M}_{\mathcal{A}}$ with the smallest norm in $\widetilde{\mathcal{F}}$. Let us start with introducing an RKHS $\mathcal{H}$ by defining a kernel function K in space $\mathcal{F}$ as in (6). Using Theorem 2.4 we find a function $f^* \in \mathcal{H}$ being the empirical risk minimizer with the smallest norm in $\mathcal{H}$, which is of the form:

$$f^*(x) = \sum_{i=1}^{k} \beta_i K(x_i, x).$$

We find the parameters $\beta_1, ..., \beta_k$ in the following manner:

$$\begin{bmatrix} \beta_1 \\ \vdots \\ \beta_k \end{bmatrix} = \begin{bmatrix} K(x_1, x_1) & \cdots & K(x_1, x_k) \\ \vdots & \ddots & \vdots \\ K(x_k, x_1) & \cdots & K(x_k, x_k) \end{bmatrix}^{-1} \begin{bmatrix} f_1 \\ \vdots \\ f_k \end{bmatrix}, \tag{13}$$

which can be written in more compact notation as

$$\boldsymbol{\beta} = \mathbf{K}^{-1} \cdot \mathbf{f}$$

with an obvious definition of terms.

Clearly, we have assumed here that *(i)* the spaces are rich enough that the error function can be minimized to zero, i.e. we can actually solve the equations $f(x_i) = f_i$, and *(ii)* that the measurements are sufficiently independent (informative) that $\mathbf{K}$ is of full order and so can be inverted. It is interesting to go beyond (i) and assume noise in the measurements which is one of the future directions we consider (see the final section). Then the invertibility of $\mathbf{K}$ in the case we are interested in, that is CSD estimation, for a

set of potential basis functions $\{b_i\}_{i=1}^n$ depends on the electrode positions $\{\mathbf{x}_i\}_{i=1}^k$. In all the cases we considered $\mathbf{K}$ turned out to be invertible and we expect this to be true for all experimentally accessible electrode setups. In general, if $\mathbf{K}$ were ill-conditioned, we would consider a richer space $\mathcal{F}$.

Having f^* given by

$$f^*(x) = \sum_{i=1}^{k} \beta_i K(x_i, x) = \sum_{i=1}^{k} \beta_i \sum_{j=1}^{n} b_j(x_i) b_j(x) \tag{14}$$

we know that there exists exactly one $\widetilde{f}^* \in \widetilde{\mathcal{F}}$ such that $\mathcal{A}\widetilde{f}^* = f^*$ and it is given by

$$\widetilde{f}^* = \sum_{i=1}^{k} \beta_i \sum_{j=1}^{n} b_j(x_i) \widetilde{b}_j(x) = \sum_{i=1}^{k} \beta_i \widetilde{K}(x_i, x). \tag{15}$$

We call

$$\widetilde{K}(x, y) = \sum_{i=1}^{n} b_i(x) \widetilde{b}_i(y) \tag{16}$$

the *cross-kernel function*. Thus, if we define the *vector* function

$$\widetilde{\mathbf{K}}^T(x) := [\widetilde{K}(x_1, x), \ldots, \widetilde{K}(x_n, x)],$$

then

$$\widetilde{f}^*(x) = \widetilde{\mathbf{K}}^T(x) \cdot \mathbf{K}^{-1} \cdot \mathbf{f}. \tag{17}$$

From (12) we see that $\widetilde{f}^*$ has the smallest norm in $\widetilde{\mathcal{F}}$.

3.2 The kCSD method

We now move from a general framework to the specific case of current source density estimation. Suppose we want to estimate current source density (CSD) from a finite set of Local Field Potential (LFP) measurements: $(x_i, f_i)_{i=1}^k, x_i \in \mathbb{R}^3$. In this section we show that the connection between the potentials recorded on the electrodes (*denoted by* f) and the CSD (*denoted by* $\widetilde{f}$) is in various cases given by a linear operator

$$\mathcal{A}\widetilde{f} = f. \tag{18}$$

We therefore conclude that our task of estimation is a special case of a linear operator equation discussed in the previous section. To give the problem its formal structure we have to define the classes $\mathcal{F}$ and $\widetilde{\mathcal{F}}$.

We first introduce $\widetilde{\mathcal{F}}$, the space of CSD by choosing its n linearly independent basis functions $\left\{\widetilde{b}_i(x)\right\}_{i=1}^n$. We do so according to our intuition on the CSD, possibly incorporating known anatomy, and we are free to choose very large n. Examples of such choices will be given in sections 3.2.1–3.2.3. In this paper we don't examine the time dependence of the potentials. CSD is estimated separately for each time frame. However, taking time into account within the CSD framework is an interesting possibility to consider in the future. In Section 5 we briefly present our ideas concerning this issue.

For every CSD basis function $\widetilde{b}_i(x')$ we calculate the potential generated by such a source at every $x \in \mathbb{R}^3$ and obtain the basis of potentials $\{b_i(x)\}_{i=1}^n$ so that for every i, $b_i = \mathcal{A}\widetilde{b}_i$. Next we define $K(x, y), \widetilde{K}(x, y)$ and find $\widetilde{f}^*$ as discussed in the previous section.

In practice, one faces a range of problems of CSD estimation from various electrode arrangements, both available commercially or home-made. In particular, electrodes are often arranged on flat surfaces (for multishaft multielectrodes or MEA) or on straight lines (for laminar multielectrodes). It is crucial to distinguish situations in which measurements are taken at positions more or less uniformly distributed in $\mathbb{R}^3$ from those, where the contacts are distributed on a lower dimensional subspace of $\mathbb{R}^3$. Below we suggest possible ways of making such distinctions. In all further sections σ will denote space conductivity, which we assume is constant.

We shall start with the simplest conceptually and numerically case of recordings in three-dimensional space (Łęski, Wójcik, Tereszczuk, Świejkowski, Kublik & Wróbel 2007), following with the discussion of 2D (Łęski, Pettersen, Tunstall, Einevoll, Gigg & Wójcik 2010) and 1D (Pettersen et al. 2006) cases.

3.2.1 kCSD in 3D

Consider a situation in which the electrodes are arranged in $\mathbb{R}^3$ in such a way that their positions can't be immersed in any one or two dimensional subspace (a line or a plane). This case includes the situation of electrodes positioned at the nodes of a regular 3D rectangular grid as in Łęski, Wójcik, Tereszczuk, Świejkowski, Kublik & Wróbel (2007). Another exemplary situation would be a random choice of electrode positions in $\mathbb{R}^3$ which could arise when positioning electrodes in a specific structure to obtain reliable single unit recordings from different cells. In order to model the CSD profile $\widetilde{f}(x, y, z)$ let us point out that the potential measured at some point (x, y, z) generated by this profile is given by:

$$f(x,y,z) = \frac{1}{4\pi\sigma}\int dx' \int dy' \int dz' \, \frac{\widetilde{f}(x',y',z')}{\sqrt{(x-x')^2+(y-y')^2+(z-z')^2}} =: (\mathcal{A}_3\widetilde{f})(x,y,z). \tag{19}$$

In this case also the Poisson equation holds:

$$\nabla(\sigma\nabla)(f) = -\widetilde{f}. \tag{20}$$

We can define spaces $\widetilde{\mathcal{F}}$ and $\mathcal{F}$ by introducing their basis functions. This can be done in various ways, we considered two cases defining the basis of the CSD space $\widetilde{\mathcal{F}}$. One basis is defined by a family of simple step functions on a ball:

$$\widetilde{b}_i(x,y,z) = \begin{cases} 1 & (x-x_i)^2+(y-y_i)^2+(z-z_i)^2 \leq R^2 \\ 0 & \text{otherwise} \end{cases} \tag{21}$$

the other by a family of Gaussians:

$$\widetilde{b}_i(x,y,z) = \exp\left(-\frac{(x-x_i)^2+(y-y_i)^2+(z-z_i)^2}{2R}\right). \tag{22}$$

In both cases the positions of centers of each basis function (x_i, y_i, z_i) were selected so as to cover the studied region uniformly, which is described in detail in Section 3.2.4. The corresponding potential basis functions b_i can be derived by applying equation (19):

$$b_i(x,y,z) = \frac{1}{4\pi\sigma}\int dx' \int dy' \int dz' \, \frac{\widetilde{b}_i(x',y',z')}{\sqrt{(x-x')^2+(y-y')^2+(z-z')^2}}. \tag{23}$$

In lower dimensionality the framework changes because in order to calculate the potentials generated by a source we must assume the structure of the source in the normal (perpendicular) directions to the plane (in 2D) or line (in 1D) of measurements. The need for such models and specific examples were carefully discussed by Pettersen et al. (2006) for the case of laminar recordings and by Łęski, Pettersen, Tunstall, Einevoll, Gigg & Wójcik (2010) for planar recordings (such as multishaft electrodes).

3.2.2 kCSD in 2D

Consider a situation in which LFP is measured by electrodes that are arranged on a flat surface, e.g. as in (Csicsvari et al. 2003). To estimate CSD we need to make assumptions about its profile in the direction perpendicular to the surface. Let's introduce a coordinate system (x, y, z) and assume that the electrodes are arranged on the surface spanned by the x and y axes. In Łęski, Pettersen, Tunstall, Einevoll, Gigg & Wójcik (2010) we proposed to consider the CSD as a product of an a priori two-dimensional profile $\widetilde{f}(x, y)$ and a specific profile H in the perpendicular direction z :

$$\widetilde{f}(x, y, z) = \widetilde{f}(x, y)H(z).$$

For $H(z)$ here we take a simple step function:

$$H(z) = \begin{cases} 1 & -h \leq z \leq h \\ 0 & \text{otherwise} \end{cases}$$

although other choices such as a Gaussian profile are also possible. Thus we assume that the CSD profile is constant in z direction within a slice of thickness $2h$ centered at the surface with electrodes and 0 elsewhere. It turns out that the specific choice of profile $H(z)$ influences mainly the amplitude of the calculated potentials and so the estimated sources, while their overall shape is reasonably robust (Łęski, Pettersen, Tunstall, Einevoll, Gigg & Wójcik 2010).

The potential measured by an electrode placed in some point $(x, y, 0)$ is in this case given by:

$$f(x, y) = \frac{1}{2\pi\sigma} \int dx' \int dy' \ \text{arsinh}\left(\frac{2h}{\sqrt{(x - x')^2 + (y - y')^2}}\right) \widetilde{f}(x', y') =: (\mathcal{A}_2\widetilde{f})(x, y). \tag{24}$$

In this case it is sufficient to estimate the two-dimensional profile $\widetilde{f}(x, y)$ to get an estimate of the overall CSD in the region. Therefore we can define spaces $\mathcal{F}$ and $\widetilde{\mathcal{F}}$ by introducing two-variable basis functions. This can be done similarly as in the 3D case, using simple step basis functions for space $\widetilde{\mathcal{F}}$:

$$\widetilde{b}_i(x, y) = \begin{cases} 1 & (x - x_i)^2 + (y - y_i)^2 \leq R^2 \\ 0 & \text{otherwise} \end{cases} \tag{25}$$

or Gaussians:

$$\widetilde{b}_i(x, y) = \exp\left(-\frac{(x - x_i)^2 + (y - y_i)^2}{2R}\right). \tag{26}$$

The potential basis functions $b_i \in \mathcal{F}$ can be derived by applying equation (24):

$$b_i(x, y) = \frac{1}{2\pi\sigma} \int dx' \int dy' \ \text{arsinh}\left(\frac{2h}{\sqrt{(x - x')^2 + (y - y')^2}}\right) \widetilde{b}_i(x', y'). \tag{27}$$

3.2.3 kCSD in 1D

Assume that the electrodes are arranged along a straight line. As in the previous section we need to make assumptions on CSD profile in the perpendicular plane. Pettersen et al. (2006) proposed to introduce an overall CSD profile of the form:

$$\widetilde{f}(x, y, z) = \widetilde{f}(z)H(x, y).$$

We assume rotational symmetry around z axis and for $H(x, y)$ we take a simple step function on a disk of radius r:

$$H(x, y) = \begin{cases} 1 & x^2 + y^2 \leq r^2, \\ 0 & \text{otherwise.} \end{cases}$$

The potential measured by an electrode placed in some point $(0, 0, z)$ is in this case given by:

$$f(z) = \frac{1}{2\sigma} \int dz' \left(\sqrt{(z - z')^2 + r^2} - |z - z'| \right) \widetilde{f}(z') = (\mathcal{A}_1 \widetilde{f})(z) \tag{28}$$

Now the space of CSD $\widetilde{\mathcal{F}}$ can be defined by introducing one-variable basis functions. As in the previous cases, one can use simple step functions

$$\widetilde{b}_i(z) = \mathbb{I}_{[z_i - R; z_i + R]}(z) \tag{29}$$

or Gaussians

$$\widetilde{b}_i(z) = \exp\left(-\frac{(z - z_i)^2}{2R} \right). \tag{30}$$

Finally, the potential basis functions $b_i \in \mathcal{F}$ can be obtained by applying equation (28):

$$b_i(z) = \frac{1}{2\sigma} \int dz' \left(\sqrt{(z - z')^2 + r^2} - |z - z'| \right) \widetilde{b}_i(z'). \tag{31}$$

3.2.4 Spatial arrangement of the basis elements

In Section 3 we introduced example shapes of the basis functions $\left\{ \widetilde{b}_i \right\}_{i=1}^{n}$ which we considered in various dimensions. To implement kCSD we have to specify the number and localization of these sources. Let us denote the area where we want to estimate CSD by $\mathcal{A} \subset \mathbb{R}^d$, where $d \in \{1, 2, 3\}$. In all the tests we carried out $\mathcal{A}$ was a product of intervals, $\mathcal{A} = \cap_{k=1}^{d} I_k$, $I_k = [a_k, b_k] \subset \mathbb{R}$, for example, in Section 4.1:

$$\mathcal{A} = \left\{ (x, y) \in \mathbb{R}^2 : x_{\min} - \xi\Delta x \leq x \leq x_{\max} + \xi\Delta x, y_{\min} - \xi\Delta y \leq y \leq y_{\max} + \xi\Delta y \right\}.$$

To generate the basis of sources we always took a spherically symmetric template function $\widetilde{b}(\mathbf{x})$ and translated it to nodes of a regular, rectangular grid $\mathbf{x}_i \in \mathcal{A}$ obtaining the full basis $\widetilde{b}_i(\mathbf{x}) = \widetilde{b}\left((\mathbf{x} - \mathbf{x}_i)^2\right)$ making sure that each point in the estimation area $\mathcal{A}$ belongs to the support of at least two basis sources. To get elegant results it turned out that R should be a multiple of the spacing between the grid nodes, otherwise we observed significant irregularities.

3.3 iCSD as a special case of kCSD

In this section we show that the inverse Current Source Density method (Pettersen et al. 2006, Łęski, Wójcik, Tereszczuk, Świejkowski, Kublik & Wróbel 2007, Łęski, Pettersen, Tunstall, Einevoll, Gigg & Wójcik 2010) is a special case of kernel Current Source Density when the assumed number of sources, n, is equal to the number of measured potentials, k.

To set the stage let us rewrite iCSD in the language used here. We start from a set of k LFP measurements: $(\mathbf{x}_i, \Phi_i)_{i=1}^k, \mathbf{x}_i \in \mathbb{R}^d$. Then a model of CSD is assumed in the form of n-parameter distribution

$$C(\mathbf{x}) = \sum_{j=1}^{n} C_j \widetilde{b}_j(\mathbf{x}).$$

In all the work so far $\mathbf{x}_i$ were assumed to form a regular rectangular grid and C_i were the values of CSD at the nodes of the grid which were to be estimated from the given potentials.

The spatial profiles $\widetilde{b}_i(\mathbf{x})$ and the associated potentials $b_i(\mathbf{x})$ are set by the dimensionality of the problem and the variant of the method used (step, linear spline, cubic spline, etc.). For example, in three dimensional spline method $\widetilde{b}_i(\mathbf{x})$ would be spline interpolated three-dimensional function between grid points, taking values 1 at $\mathbf{x}_i$ and 0 at $\mathbf{x}_{j\neq i}$ with appropriate boundary conditions (Łęski, Wójcik, Tereszczuk, Świejkowski, Kublik & Wróbel 2007). The potential generated by source $\widetilde{b}_i(\mathbf{x})$ is given by Eq. (23).

In lower dimensionality one has to add a model of sources in the directions not probed by the electrodes. Thus in the two-dimensional step method (Łęski, Pettersen, Tunstall, Einevoll, Gigg & Wójcik 2010), for example, assuming $\mathbf{x}_i \equiv (x_i, y_i, 0)$ with interelectrode distance Δ and step profile in the perpendicular direction of the depth H we would have

$$\widetilde{b}_i(x, y, z) = \begin{cases} 1 & x \in (x_i - \frac{\Delta}{2}, x_i + \frac{\Delta}{2}), y \in (y_i - \frac{\Delta}{2}, y_i + \frac{\Delta}{2}), z \in (-\frac{H}{2}, \frac{H}{2}) \\ 0 & \text{otherwise} \end{cases}$$

with the potentials given by Eq. (27).

In any iCSD variant, the potentials according to the assumed model of sources are given by

$$\Phi(\mathbf{x}) = \sum_j C_j b_j(\mathbf{x})$$

with the values measured at a grid point i equal to

$$\Phi(\mathbf{x}_i) = \sum_j C_j b_j(\mathbf{x}_i) = \Phi_i.$$

To find the model sources we first solve for parameters C_j given the potentials:

$$\Phi \equiv \begin{bmatrix} \Phi_1 \\ \vdots \\ \Phi_k \end{bmatrix} = \begin{bmatrix} b_1(\mathbf{x}_1) & \dots & b_n(\mathbf{x}_1) \\ & \vdots & \\ b_1(\mathbf{x}_k) & \dots & b_n(\mathbf{x}_k) \end{bmatrix} \begin{bmatrix} C_1 \\ \vdots \\ C_n \end{bmatrix} = \begin{bmatrix} \mathbf{b}^T(\mathbf{x}_1) \\ \vdots \\ \mathbf{b}^T(\mathbf{x}_k) \end{bmatrix} \begin{bmatrix} C_1 \\ \vdots \\ C_n \end{bmatrix}$$

with obvious notation

$$\mathbf{b}(\mathbf{x}) = \begin{bmatrix} b_1(\mathbf{x}) \\ \vdots \\ b_n(\mathbf{x}) \end{bmatrix}.$$

Since in iCSD we have $n = k$ and the functions $b_j(x)$ are linearly independent we can invert this relation obtaining

$$C = \begin{bmatrix} C_1 \\ \vdots \\ C_n \end{bmatrix} = \begin{bmatrix} \mathbf{b}^T(x_1) \\ \vdots \\ \mathbf{b}^T(x_k) \end{bmatrix}^{-1} \Phi.$$

Then the source are given by

$$C_{\mathrm{iCSD}}(\mathbf{x}) = \sum_{j=1}^{n} C_j \widetilde{b}_j(\mathbf{x}) = \widetilde{\mathbf{b}}^T(x) \begin{bmatrix} \mathbf{b}^T(\mathbf{x}_1) \\ \vdots \\ \mathbf{b}^T(\mathbf{x}_k) \end{bmatrix}^{-1} \Phi. \tag{32}$$

In kCSD framework we have (Eq. (14)):

$$\begin{aligned} \begin{bmatrix} \Phi_1 \\ \vdots \\ \Phi_k \end{bmatrix} &= \begin{bmatrix} K(\mathbf{x}_1, \mathbf{x}_1) & \dots & K(\mathbf{x}_1, \mathbf{x}_k) \\ & \vdots & \\ K(\mathbf{x}_k, \mathbf{x}_1) & \dots & K(\mathbf{x}_k, \mathbf{x}_k) \end{bmatrix} \begin{bmatrix} \beta_1 \\ \vdots \\ \beta_k \end{bmatrix} \\ &= \begin{bmatrix} \sum_{j=1}^n b_j(\mathbf{x}_1) b_j(\mathbf{x}_1) & \dots & \sum_{j=1}^n b_j(\mathbf{x}_1) b_j(\mathbf{x}_k) \\ & \vdots & \\ \sum_{j=1}^n b_j(\mathbf{x}_k) b_j(\mathbf{x}_1) & \dots & \sum_{j=1}^n b_j(\mathbf{x}_k) b_j(\mathbf{x}_k) \end{bmatrix} \begin{bmatrix} \beta_1 \\ \vdots \\ \beta_k \end{bmatrix} \\ &= \begin{bmatrix} \mathbf{b}^T(\mathbf{x}_1) \\ \vdots \\ \mathbf{b}^T(\mathbf{x}_k) \end{bmatrix} \begin{bmatrix} \mathbf{b}(\mathbf{x}_1) & \dots & \mathbf{b}(\mathbf{x}_k) \end{bmatrix} \begin{bmatrix} \beta_1 \\ \vdots \\ \beta_k \end{bmatrix} \end{aligned}$$

Again, since we assumed $n = k$ we can invert both matrices to obtain

$$\begin{bmatrix} \beta_1 \\ \vdots \\ \beta_k \end{bmatrix} = \begin{bmatrix} \mathbf{b}(\mathbf{x}_1) & \dots & \mathbf{b}(\mathbf{x}_k) \end{bmatrix}^{-1} \begin{bmatrix} \mathbf{b}^T(\mathbf{x}_1) \\ \vdots \\ \mathbf{b}^T(\mathbf{x}_k) \end{bmatrix}^{-1} \Phi. \tag{33}$$

Then the sources $C_{\mathrm{kCSD}}(x)$ according to Eq. (15) are given by

$$\begin{aligned} C_{\mathrm{kCSD}}(x) &= \sum_{i=1}^{k} \beta_i \sum_{j=1}^{n} b_j(\mathbf{x}_i) \widetilde{b}_j(\mathbf{x}) \\ &= \begin{bmatrix} \sum_j \widetilde{b}_j(\mathbf{x}) b_j(\mathbf{x}_1) & \dots & \sum_j \widetilde{b}_j(\mathbf{x}) b_j(\mathbf{x}_k) \end{bmatrix} \begin{bmatrix} \beta_1 \\ \vdots \\ \beta_k \end{bmatrix} \\ &= \widetilde{\mathbf{b}}^T(\mathbf{x}) \begin{bmatrix} \mathbf{b}(\mathbf{x}_1) & \dots & \mathbf{b}(\mathbf{x}_k) \end{bmatrix} \begin{bmatrix} \beta_1 \\ \vdots \\ \beta_k \end{bmatrix} \end{aligned} \tag{34}$$

Using (33) and (34) we obtain

$$
\begin{aligned}
C_{\mathrm{kCSD}}(x) &= \widetilde{\mathbf{b}}^T(\mathbf{x}) \left[\begin{array}{ccc} \mathbf{b}(\mathbf{x}_1) & \dots & \mathbf{b}(\mathbf{x}_k) \end{array} \right] \left[\begin{array}{ccc} \mathbf{b}(\mathbf{x}_1) & \dots & \mathbf{b}(\mathbf{x}_k) \end{array} \right]^{-1} \left[\begin{array}{c} \mathbf{b}^T(\mathbf{x}_1) \\ \vdots \\ \mathbf{b}^T(\mathbf{x}_k) \end{array} \right]^{-1} \Phi \\
&= \widetilde{\mathbf{b}}^T(\mathbf{x}) \left[\begin{array}{c} \mathbf{b}^T(\mathbf{x}_1) \\ \vdots \\ \mathbf{b}^T(\mathbf{x}_k) \end{array} \right]^{-1} \Phi \\
&= C_{\mathrm{iCSD}}(\mathbf{x}). \qquad (35)
\end{aligned}
$$

4 Tests and examples

To test the viability of the kCSD method we performed a number of numerical experiments using model sources and experimentally registered potentials.

The first question is how the kCSD method compares to the other methods (finite-difference approximation, inverse CSD). To answer this we used several configurations of the model CSD to calculate the potentials which would have been measured using multi-contact electrodes. To be able to apply all the different CSD methods we had to use regular grids, that means we calculated the potentials either at equidistant points in 1D or at points which formed a Cartesian grid in 2D or 3D. Then we tested the similarity of the CSD reconstructions to the model CSD for a wide range of parameters of the kCSD method. These tests are described in more detail in Section 4.1 below. The conclusion is that for the electrode grids where all the methods can be applied the kCSD method performs as well as the spline iCSD method or better (which is typically better than the finite difference — 'traditional' — CSD analysis) if we choose basis appropriately.

A major strength of kCSD is its capability to estimate CSD from arbitrary distributions of contacts with equal ease. Thus the second and perhaps the most interesting question is how the kCSD method performs for contacts not forming a regular grid. Though it is sometimes possible to use other CSD methods in such cases, it is usually harder to use them without the assumption of the regularity and the kCSD method seems to be the most natural choice. We illustrate this below in Section 4.2. First we show how the kCSD method can be easily applied to (model) potentials recorded on a grid used in Wirth & Lüscher (2004). Then we test the quality of reconstruction for electrodes placed randomly within the probed area and check how it changes with increasing number of electrodes.

The intermediate case between regular and irregular grids is when we use a grid of regularly placed contacts but with a small number of contacts missing. This can happen, for example, when one or two contacts are used for stimulation instead of recording. This problem was studied earlier in Wójcik & Łęski (2010) where two approaches based on iCSD were proposed: one was to substitute the missing channels with averages of their neighbors (LA for local averages), the other was to restrict the dimensionality of the possible CSD distributions and use the least-squares fit to all available recordings (LS). Again, the kCSD method seems to be a natural choice here. In Section 4.3 we test the kCSD method on the same experimental data as used in Wójcik & Łęski (2010) and show that it is a substantially better approach than the LS method from Wójcik & Łęski (2010). Comparison of kCSD with the LA method depends on the dataset tested.

4.1 Comparison of CSD methods on regular grids

The kCSD method as defined above has a number of parameters which need to be specified before the method can be applied to data. Specifically, we need to define the basis $\left\{\widetilde{b}_i(x)\right\}_{i=1}^{n}$ of the space of the CSD distributions $\widetilde{\mathcal{F}}$. As an example we will consider a two-dimensional regular, rectangular electrode grid ($z = 0$ for all electrodes). We generate all the basis functions by translating a single reference function of the form $c(x, y)H(z)$ where as in Section 3.2.2 for $c(x, y)$ we take either a two-dimensional Gaussian

$$c_g(x, y) = \exp\left(-\frac{x^2 + y^2}{2R}\right), \tag{36}$$

or a two-dimensional cylindrically symmetric step function

$$c_s(x, y) = \begin{cases} 1 & \text{if} \quad x^2 + y^2 < R^2 \\ 0 & \text{otherwise.} \end{cases} \tag{37}$$

Therefore, each basis function $\widetilde{b}_i$ is a translation of c_s or c_g. The parameter R in the formulae above is the size of the basis sources in the xy plane. As the transverse profile $H(z)$ we take a step function: $H(z) = 1$ for $-h \leq z \leq h$. Let $x_{\min}, x_{\max}$ denote the minimum and the maximum of the x coordinates of the electrodes, similarly for y; the spacing of the grid is $\Delta x, \Delta y$. We assume that the sources can extend beyond the electrode grid, specifically, the central points (x, y) of the basis functions can be in the region $x_{\min} - \xi\Delta x \leq x \leq x_{\max} + \xi\Delta x$, $y_{\min} - \xi\Delta y \leq y \leq y_{\max} + \xi\Delta y$, where ξ is a parameter. We arrange the sources as described along a regular rectangular grid. The final parameter is the number of sources n. We choose such n that it is a product of numbers of equally spaced sources in x and y directions. Summarizing, the parameters we have to specify are n, R, h, and ξ, and the choice between step and Gaussian profiles in the xy plane. The choice of the translation parameters and number of sources was described in Section 3.2.4.

Let us focus on an eight-by-eight grid with equal spacing in both directions ($\Delta x = \Delta y = 0.2$, all lengths in this section are in mm) spanning the area $0 \leq x, y \leq 1.4$. We chose two sets of test sources, both having product structure $c(x, y)H(z)$ with $H(z) = 1$ for $-0.5 \leq z \leq 0.5$. The datasets are composed of Gaussian sources: in the first set the sources are large compared to the inter-electrode distance (Fig. 1A), and in the second dataset they are small (Fig. 2A). The exact formulae are given in the Appendix B.

We calculated the potentials at the registration points (for that purpose the integration area was $(x, y) \in [-0.5, 1.9] \times [-0.5, 1.9]$). Then we performed a scan over the space of parameters of the kCSD method: we took all possible combinations of $R = 0.05, 0.1, 0.15, \ldots, 0.4$, $n = 90^2, 120^2, \ldots, 240^2$, $h = 0.2, 0.5, 1$, and $\xi = 0, 0.5, 1, 2, 3$. For each combination of parameters, and for both the Gaussian and the step profiles we reconstructed the CSD and calculated the normalized reconstruction error e using the formula

$$e = \frac{\int (c(x, y) - \hat{c}(x, y))^2}{\int c(x, y)^2},$$

where $\hat{c}(x, y)$ is the reconstructed CSD (Łęski, Wójcik, Tereszczuk, Świejkowski, Kublik & Wróbel 2007).

In Figures 1 and 2

we show example reconstructions using the kCSD method with parameters close to optimal (Fig. 1E, Fig. 2E) and with parameters farther from optimal (Fig. 1F, Fig. 2F),

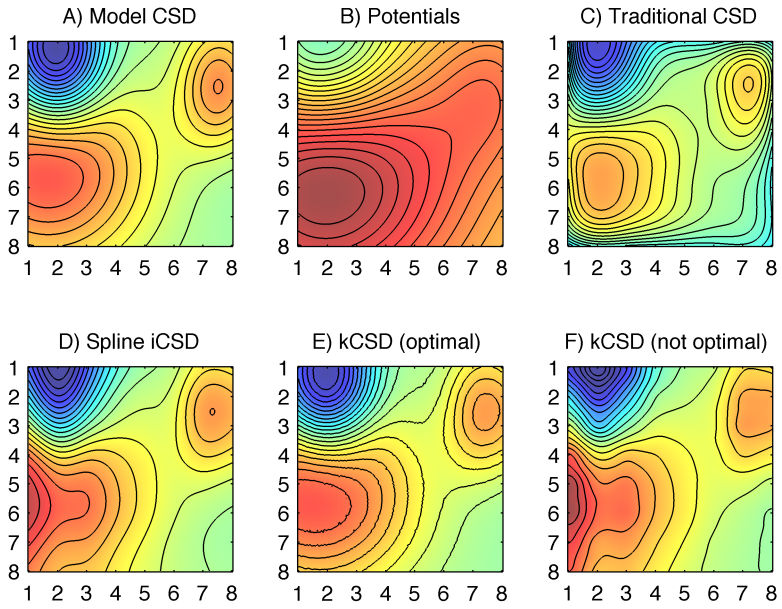

Figure 1: Test results for the first model dataset ('large sources'). A) The model CSD. B) The potentials. C) Reconstruction using traditional CSD. D) Reconstruction using spline iCSD method with D boundary conditions. E) Reconstruction using the kCSD method for $n = 8100$, $\xi = 2$, $R = 0.3$, $h = 0.5$, step z-profile. F) Reconstruction using the kCSD method for $n = 8100$, $\xi = 1$, $R = 0.1$, $h = 0.5$, Gaussian z-profile.

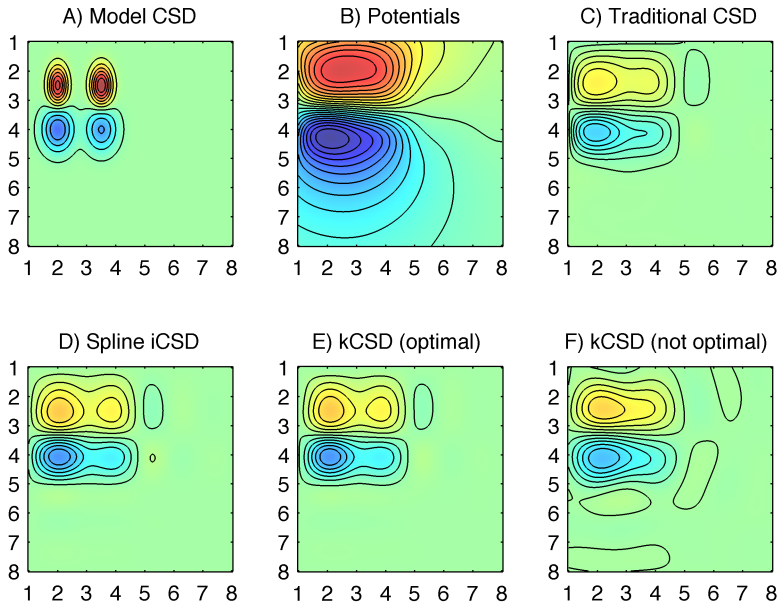

Figure 2: Test results for the first model dataset ('small sources'). A) The model CSD. B) The potentials. C) Reconstruction using traditional CSD. D) Reconstruction using spline iCSD method with D boundary conditions. E) Reconstruction using the kCSD method for $n = 8100$, $\xi = 0.5$, $R = 0.2$, $h = 0.5$, Gaussian z-profile. F) Reconstruction using the kCSD method for $n = 8100$, $\xi = 0.5$, $R = 0.4$, $h = 0.5$, Gaussian z-profile.

exact parameter sets given in captions. These are compared with traditional CSD (Fig. 1C, Fig. 2C) and spline iCSD reconstructions (Fig. 1D, Fig. 2D).

By 'traditional CSD' here and in the following we understand the following procedure: *(i)* extend the grid by extra layer in each direction and copy the potential value at extra points from nearest neighbors; *(ii)* calculate the CSD value at the grid points by discrete numerical approximation to the Laplacian; *(iii)* cubic spline interpolate in between. The iCSD with D boundary conditions means the CSD model where the original grid was extended with an extra layer and the same CSD value was assumed as in the nearest neighbor, spline interpolated CSD between the nodes (Łęski, Wójcik, Tereszczuk, Świejkowski, Kublik & Wróbel 2007, Łęski, Pettersen, Tunstall, Einevoll, Gigg & Wójcik 2010).

The errors for optimal kCSD parameters ($e = 0.06\%$ and $e = 35\%$ for large and small sources, respectively) are smaller than the errors of the traditional CSD ($e = 43\%$ and $e = 38\%$) and spline iCSD ($e = 1\%$ and $e = 36\%$). If the parameters are farther from the optimal set the error of the kCSD method grows ($e = 3\%$ and $e = 66\%$ for the presented examples). Note that for the 'small sources' data set all errors are rather large. This is because the electrodes grid is too sparse to probe the detailed structure of the sources, compare Figure 2C–F with Figure 5 where a denser electrodes grid leads to much better reconstruction. This is intuitively very natural as it resembles the situation in Fourier analysis where it is impossible to recover frequencies higher than half the sampling rate of the signal (Nyquist theorem).

The results of the parameters space scan can be summarized as follows: the most important parameter is the size of the basis sources R. For the first set of model sources ('large sources') it is best to choose large R ($R = 0.4$ or even larger), while for the second set ('small sources') the results are best for small R (~ 0.1). This is not surprising since any CSD estimation method works best if the assumed CSD family matches closely the actual distribution.

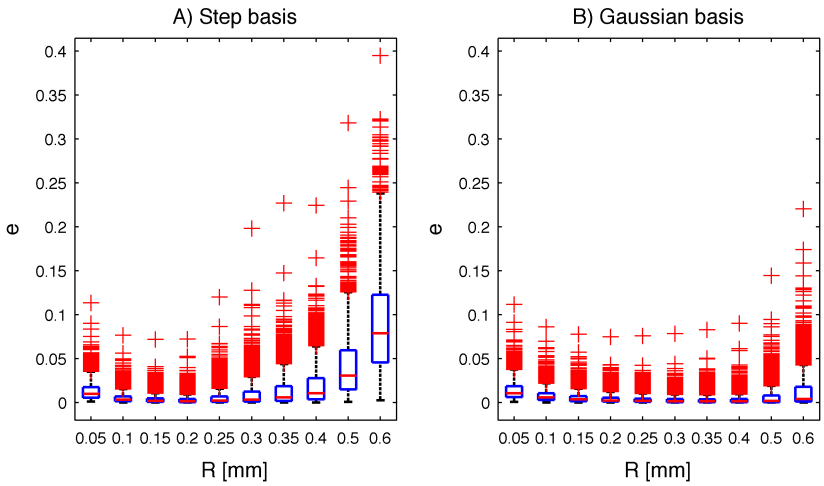

Figure 3: Dependence of reconstruction error on R for step (A) and Gaussian (B) basis sources. The boxes in the 'box and whisker' plots show the median and the lower and upper quartile values; the whiskers extend over the neighboring values up to a maximum of 1.5 times the interquartile range; the values further away are shown as outliers (+ signs, typically less than 10% of the data points).

Since optimal reconstruction parameters depend on the dataset we further tested the

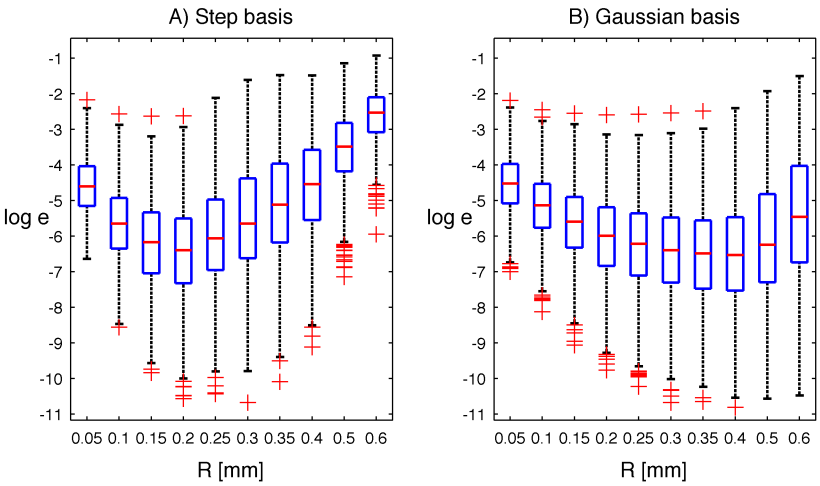

Figure 4: Dependence of (logarithm of) reconstruction error on R for step (A) and Gaussian (B) basis sources. The boxes in the 'box and whisker' plots show the median and the lower and upper quartile values; the whiskers extend over the neighboring values up to a maximum of 1.5 times the interquartile range; the values further away are shown as outliers (+ signs, typically less than 10% of the data points).

dependence of reconstruction error on R on a large set of randomly placed Gaussian sources of different sizes from small to large. We used 2000 data sets, the details on how the sources were chosen are given in the Appendix B. For each data set we performed reconstructions for different R (other parameters kept fixed). The results for both Gaussian and step bases are presented in Fig. 3 and 4. For this collection of 2000 data sets the optimal R is ~ 0.3 to 0.4 for the Gaussian basis and ~ 0.15 to 0.2 for the step basis. One interesting observation is that the Gaussian basis leads to weaker dependence of the reconstruction error on R. Therefore, the recommendation for this electrode grid would be to use Gaussian basis sources and an intermediate value of R, say $R = 0.35$. For such choice the method should work reasonably well for a wide range of CSD sources.

The conclusions regarding the choice of h are the same as in inverse CSD method (Łęski, Pettersen, Tunstall, Einevoll, Gigg & Wójcik 2010): the closer we are to the actual h, the better; assuming wrong h may have strong influence on the amplitude of the reconstructed sources but the shape of the distribution is roughly preserved. The non-zero values of the parameter ξ dramatically help in cases where the actual activity in the xy plane extends beyond the electrodes grid (the 'large sources' case). The reconstruction error grows with ξ when there is no activity beyond the grid, but this effect is very small, therefore $\xi = 1$ is a safe choice in any case. The number of sources (originally between $n = 90^2$ up to $n = 240^2$) had almost no effect on the reconstructions. We further studied reconstructions with smaller number of sources ($n = 10^2, 11^2, \ldots 15^2, 20^2, 30^2, 45^2, 60^2, 75^2$) and we found that the reconstructions only break for very sparse bases (such as $n = 10^2$); taking $n = 20^2$ yields errors only slightly higher than the optimal values of n. The reason that the method does not work for very small n (especially when used together with small R) is that the character of the cross-kernel functions changes dramatically: for larger n they are 'smooth' functions with a single maximum, whereas for small n the kernels have multiple maxima located at the observation points and are therefore unable to reproduce smooth CSD distributions faithfully. Our recommendation is that n should be such that the basis sources are denser than the observation points (for example $n = 20^2$ for 8 by 8 grid).

4.2 kCSD on irregular grids

One of the strengths of the kCSD method is that it can be easily applied to any configuration of the recording points. As an example let us consider an electrode array used by Wirth & Lüscher (2004), see Fig. 5. The contacts of the array do not form a regu-

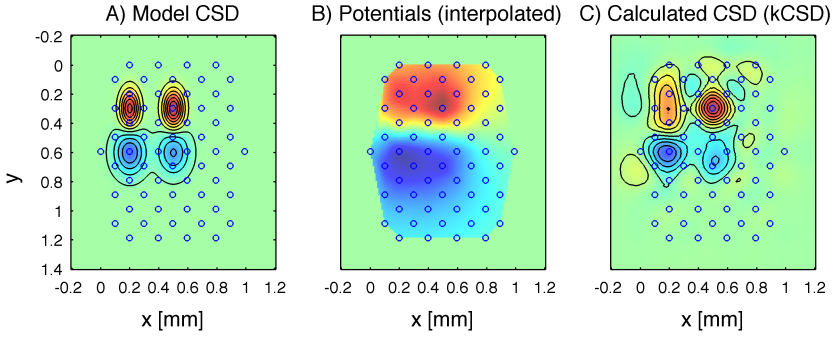

Figure 5: CSD reconstruction on an irregular grid of electrodes (circles). A) The model CSD. B) The estimated potentials. C) CSD reconstructed from potential values at the grid using kCSD method.

lar, rectangular grid similar to the ones used in Section 4.1 (although locally they form a square lattice). While it would be possible to apply some form of inverse CSD (or even numerical second derivative), the kCSD method is the most natural method to use in this case. Figure 5 presents the test sources used in this case ('small sources' dataset described in Section 4.1), the potentials resulting from the sources and the reconstructed CSD. Note that this reconstruction is better than the reconstructions obtained in Section 4.1 because the inter-electrode distance, 140μm, is smaller here.

In fact, it is equally easy to apply the kCSD method to regular and irregular grids, which is not the case for other CSD methods such as spline iCSD introduced previously. To demonstrate the strength of this new approach we consider electrodes placed *randomly*. Such irregular placement could occur in real experiments, for example, when many electrodes are positioned independently to record spiking activity and then also the LFP signal is recorded. For the two test datasets defined in Section 4.1 we chose randomly a set of electrodes placed within the area $(x, y) \in [0, 1.4] \times [0, 1.4]$ [1] and calculated the reconstruction error e (example reconstructions shown in Figure 6). For each number of electrodes we repeated this procedure 50 times to obtain error bars on e. The results are presented in Figure 7. For 'large sources' the CSD can be reconstructed quite faithfully from as little as 16 electrodes. Because of small spatial extent of 'small sources', the errors are large ($\sim 40\%$) even for 64 electrodes.

Similar reconstructions from randomly placed electrodes can be performed also in one and three dimensions. Figure 8 shows an example of reconstruction of sources (A) from 9 electrodes placed randomly on a line (B). Fig. 8 (C) shows reconstructed sources for

[1] The only constraint was that any two electrodes can not be closer than 0.14 mm.

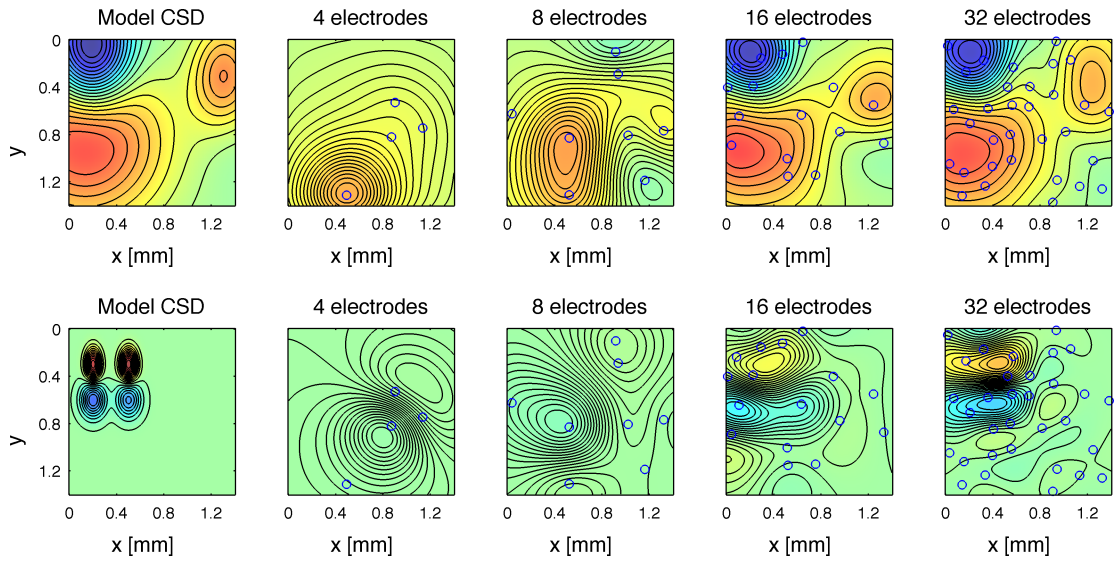

Figure 6: CSD reconstructions from randomly placed electrodes (examples). Top row: 'large sources', bottom row: 'small sources'.

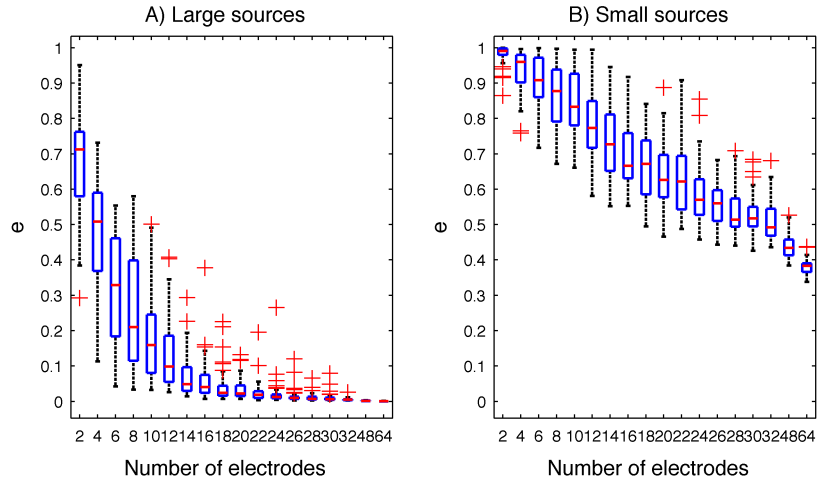

Figure 7: Distribution of errors for reconstruction from randomly placed electrodes. A) Large sources, B) small sources. For the meaning of the 'box and whisker' plots see caption of Figure 3.

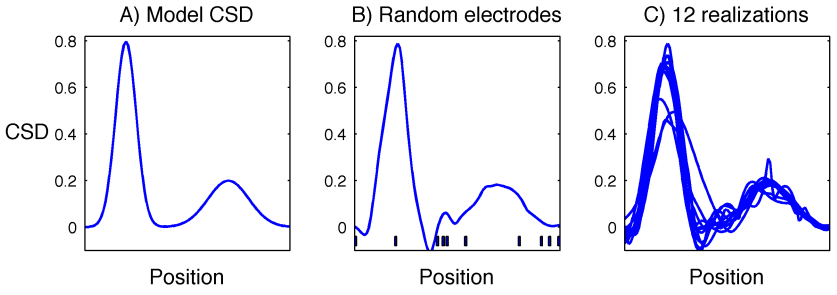

Figure 8: CSD reconstruction from randomly placed electrodes in 1D. A) model CSD; B) single reconstruction, electrodes positions are marked with vertical bars at the x axis; C) reconstructions for 12 different sets of randomly placed electrodes.

12 different distributions of nine contacts. The sources used in Fig. 8 and Fig. 9 are described in Appendix B.4.

4.3 Kernel CSD on incomplete regular grids

One interesting case of irregular grids are regular grids with a number of missing contacts. Such situations arise often in real experiments e.g. because of specific experimental setup (Bakker et al. 2009) or hardware failures. In the kCSD framework one can deal with such situations without problems. Figure 9 shows a simple one-dimensional example for the same sources presented in Fig. 8.

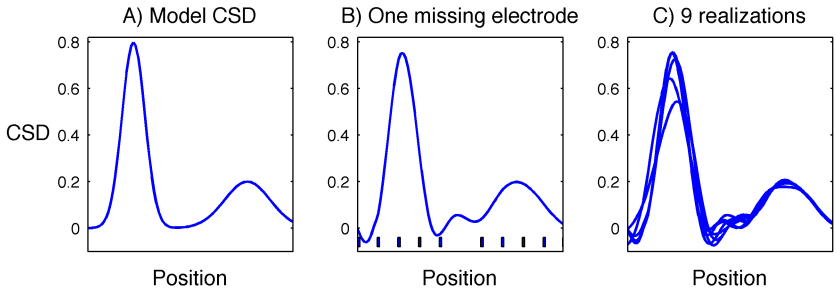

Figure 9: One-dimensional example of reconstructing CSD from a regular grid with one missing electrode. A) Model CSD. B) Reconstruction from all but one channels, electrodes positions are marked with vertical bars at the x axis — note one is missing. C) Realizations for different electrodes removed.

In previous work (Wójcik & Łęski 2010) we studied possible remedies to the 'incomplete grid' problem in the context of the inverse CSD (iCSD) method. We proposed two solutions: either to substitute the missing channels with averages of the neighbors (LA for 'local averaging') or to fit a CSD distribution described by fewer parameters than the number of electrodes using least squares method (LS). Here we treat the same problem in the context of kCSD. The kCSD method is a natural replacement for the LS approach. It can also be applied to the full dataset obtained with the LA method (the results are very close to the LA + spline iCSD method). In this section we compare the two approaches (either kCSD on incomplete grid or LA + kCSD). As the irregularity of the grid is naturally accounted for in the kCSD method without the need to explicitly use least squares fit we expect this method to perform much better than the LS method in the inverse CSD case.

To test the relative performance of kCSD and LA + kCSD methods we first studied the two-dimensional datasets ('large sources' and 'small sources') introduced above in Section 4.1. We set a number n of missing channels ($1 \leq n \leq 8$) and we studied a large number of possible combinations of missing points (for $n = 1$ and $n = 2$ we checked all possibilities, 64 and $(64 \times 63) \div 2 = 2016$, respectively; for each larger n we chose randomly 2000 combinations). For each configuration and each of the two datasets we reconstructed the CSD twice, first using the kCSD method on the incomplete dataset, second using the LA + kCSD approach. The results plotted as the mean of the reconstruction error $e \pm$ standard deviation are presented in Figure 10. The kCSD method applied to the incomplete set yields better results than the LA + kCSD method. The difference is striking in case of 'large sources', Figure 10A, which is not unexpected as we saw before that for this dataset the kCSD reconstructions are very precise even for a much smaller

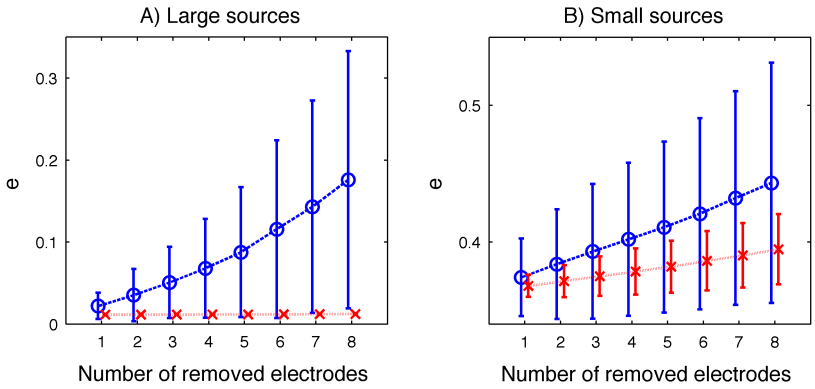

Figure 10: Comparison of two methods (LA followed by kCSD — o's, kCSD on an incomplete grid — x's) to reconstruct CSD from data on a grid with missing points. A) Large sources, B) small sources. The x-axis shows the number of recording points removed from the grid. The values plotted at y-axis are the means of normalized reconstruction error e, error bars are $\pm$ standard deviation.

number of available measurements (Figure 7). Evidently in this case local averages of neighbors lead to incorrect approximation of the missing values of potential distorting the data and resulting in bigger reconstruction errors.

To directly compare the new kCSD method to the LA + iCSD and LS methods from Wójcik & Łęski (2010) we performed another numerical experiment, this time using the experimental datasets utilized in Wójcik & Łęski (2010). The data are the extracellular evoked potentials recorded in the rat brain on a three-dimensional grid of $4 \times 5 \times 7$ points and are described in detail elsewhere (Łęski, Wójcik, Tereszczuk, Świejkowski, Kublik & Wróbel 2007, Łęski, Kublik, Świejkowski, Wróbel & Wójcik 2010). For the readers' convenience the spline iCSD reconstruction of the two time frames used here are presented in Figure 11. In Wójcik & Łęski (2010) we concluded that the LA + iCSD method is to be preferred over the less stable LS approach. Here, similarly as in the two-dimensional case above we calculated the reconstruction error for different electrodes setups using either kCSD or LA + kCSD approach[2]. As expected, the kCSD method is indeed much better than LS combined with spline iCSD: the errors of reconstruction are much smaller and the results are much more robust (there are no cases of huge errors as opposed to the LS method in Wójcik & Łęski (2010)). Still, the LA + kCSD method performs better for this datasets than pure kCSD. This is a result similar to the one obtained in Wójcik & Łęski (2010) and it is different from the result for the two-dimensional case of 'large' and 'small' sources. The results are presented in Figures 12 and 13 (the A and B panels of these figures are direct counterparts of panel C and D of figures 4 and 6 from Wójcik & Łęski (2010)).

Summarizing the two tests described above: the relative performance of the pure kCSD method on an incomplete grid vs. LA + kCSD method depends on the exact geometry of the electrodes. Therefore, we recommend that the decision if missing values should be supplemented with local averages of the neighbors is made based on tests on plausible model data for every particular electrodes setup.

[2]Note that here we know only the potentials and not the true sources, therefore the error is the difference between the reconstruction from complete and incomplete data.

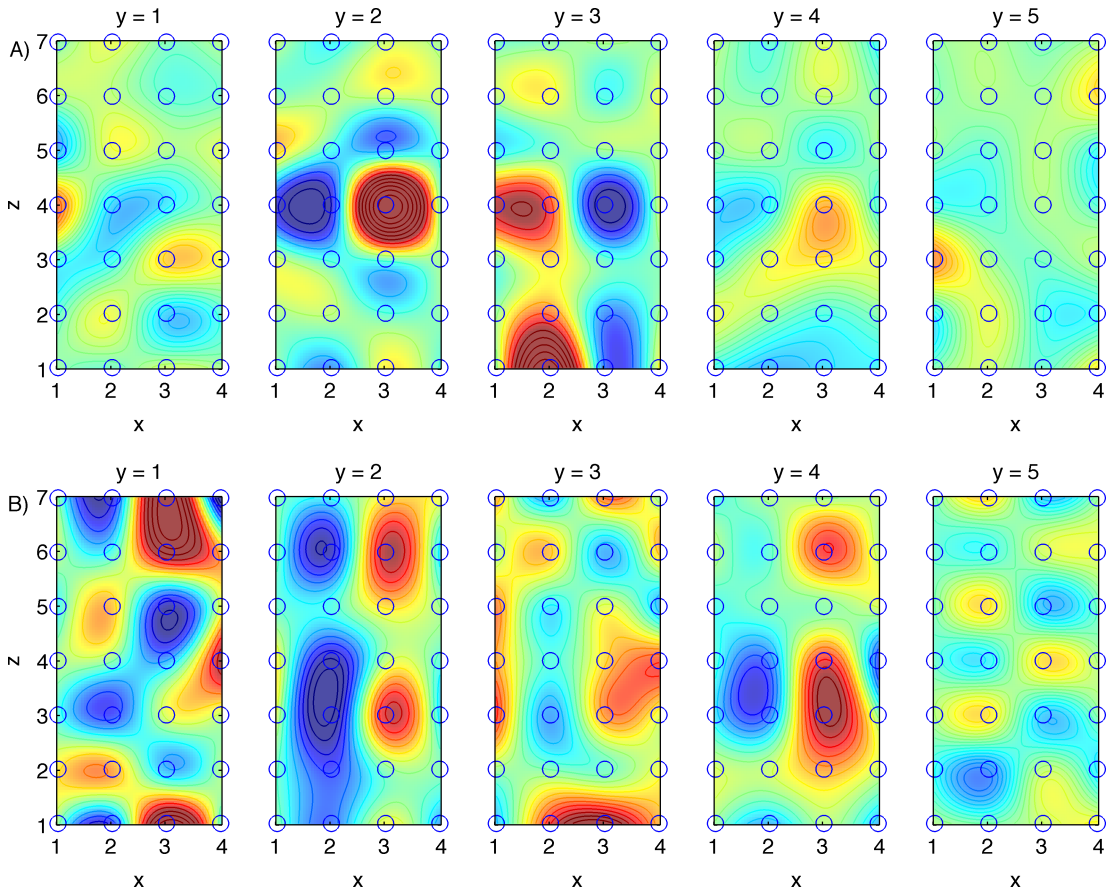

Figure 11: Experimental datasets — CSD reconstructions from complete sets of recordings. Each row presents a three-dimensional volume at a fixed time (top row: $t = 3.5$ ms, bottom row: $t = 15$ ms) after stimulus as a collection of five parallel planes. The electrodes ($4 \times 5 \times 7$ grid) are marked with circles. For details on experiment and full specification of data and procedures used see Łęski, Wójcik, Tereszczuk, Świejkowski, Kublik & Wróbel (2007).

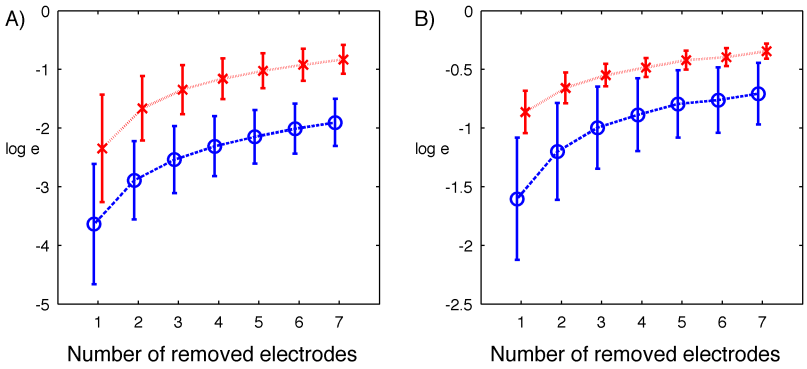

Figure 12: Comparison of two methods (LA followed by kCSD — o's, kCSD on an incomplete grid — x's) to reconstruct CSD from data on a grid with missing points. The x-axis shows the number n of recording points removed from the grid. The values plotted at y-axis are the average logarithm of normalized reconstruction error e, error bars are $\pm$ standard deviation. (A) The best 90% out of 2000 random choices of removed points (except $n = 1$ and $n = 2$ where 90% of all possibilities are used). (B) Same as (A) but for the worst 10% of the cases. The data used here are the same as used in Figures 3 and 4 in Wójcik & Łęski (2010), see also Figure 11A above.

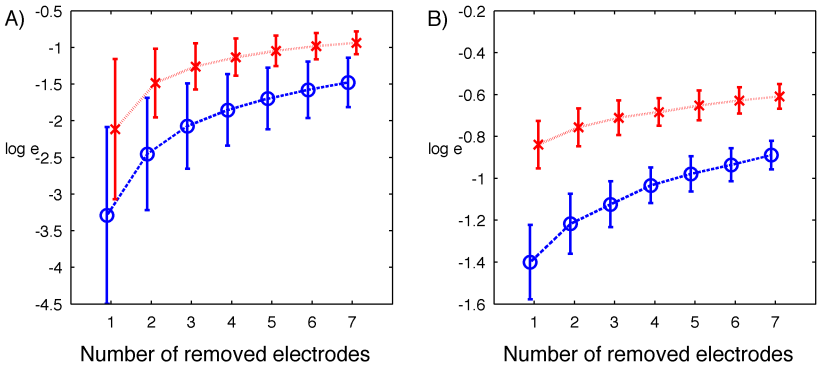

Figure 13: Comparison of methods of reconstructing CSD from incomplete data; see the caption of Figure 12. The data used here are the same as used in Figures 5 and 6 in Wójcik & Łęski (2010), see also Figure 11B above.

5 Discussion and summary

In this article we have introduced a new framework for estimation of current sources from recorded extracellular potentials using kernel methods. Introduction of kernels in this context opens up new experimental possibilities allowing efficient approximation of the sources from arbitrary distributions of contacts. We discuss here the advantages and limitations of the presented approach indicating possible further directions of development, both in the physical and statistical aspects of the problem.

Advantages of kCSD The main advantages of kCSD compared with the previously developed methods are *(i)* conceptual separation of the model construction (introducing the sources and potentials — the $b_i(x)$ and $\widetilde{b}_j(y)$ basis functions) from the distribution of electrode locations, and *(ii)* ease of reconstructing CSD from arbitrarily located contacts. One immediate benefit is that in cases such as the 3D recordings analyzed in Łęski, Wójcik, Tereszczuk, Świejkowski, Kublik & Wróbel (2007), Łęski, Kublik, Świejkowski, Wróbel & Wójcik (2010), where we know that the potentials where not recorded *exactly* on a grid, in the framework of kCSD we can take the best estimates of electrode position and the cost of calculations does not change, as opposed to the 3D iCSD where we assumed electrode location on a regular grid and neglected possible errors.

This flexibility may lead to new experimental possibilities. One case we see is combining acute experiments, such as the one described in Łęski, Wójcik, Tereszczuk, Świejkowski, Kublik & Wróbel (2007), Łęski, Kublik, Świejkowski, Wróbel & Wójcik (2010), where one can perform precise scans of electrical activation of tissue with high spatial resolution, with chronic experiments, were of necessity, one would restrict himself to a few precisely positioned electrodes, usually not on a grid. One could then use the information about the activity of CSD obtained in the acute experiments to build optimal model spaces allowing the best possible reconstruction of the sources from the limited number of measurements available in the chronic situation. This may lead to a clearer spatial and temporal separation of functional pathways than possible using methods available so far.

Interplay of modeling and data analysis in CSD reconstruction A question which arises in connection with the above mentioned approach is this: given a specific profile of the sources, including their temporal dynamics or not, assume available K electrodes. How

should they be positioned and how should one construct the model RKHS to minimize errors of CSD reconstruction in the studied process? Or alternatively, how many electrodes are needed and how should they be positioned to allow for efficient estimation of CSD with given precision? We expect that the answers to these open questions would significantly depend on the specific activity and structure. To find optimal positions for recording it would probably be necessary to test different arrangements of electrodes on simulated data. This calls for a new optimization scheme and for development of efficient simulations of local field potentials in realistic geometries.

Spectral decomposition We have concentrated here on the estimation of sources from potentials, as the CSD seems to be the main object of interest in terms of physiology. However, the approach through RKHS can give us additional insight through the 'spectral decomposition' (Shi et al. 2008). That is, for a selected representation of sources (given set of basis sources $\widetilde{b}_i(x)$) we can calculate the contribution of every basis source to the estimated CSD at any time point. We can write Eq. (17) as

$$\widetilde{f}^*(x) = \sum_{j=1}^{n} \alpha_j \widetilde{b}_j(x)$$

where

$$\alpha_j = \sum_{i=1}^{k} \beta_i b_j(x_i).$$

It may happen that temporal changes of 'activation' α_j of a source $\widetilde{b}_j(y)$ centered on x_j are different from the value of estimated CSD at x, as this is a sum of contributions from all the sources $\widetilde{b}_i$ containing x_j in their support. This could yield additional insight in the analysis of data, especially if the construction of the underlying RKHS is motivated anatomically and the basic sources can be attributed functional meaning.

Parameter choice for kCSD The kCSD framework which we have introduced here is very flexible, one can use many different types of bases. This leads to a question what is the recommended first choice of model space and how to choose parameters for unknown sources. As our numerical experiments in Section 4 show, Gaussian models give smaller errors in a larger range of parameters than the step functions, so we recommend the Gaussians. The optimal value of R for electrodes on regular grid is between 1-2 inter-electrode distances. We expect that even better results can be obtained with basis adapted to problem at hand. Its construction should be motivated by available anatomical and functional information or tests on sources generated in computational modeling, if only possible. Efficient construction of optimal basis for a problem at hand is another another direction worth exploring.

Including time dependence As mentioned in Section 3 time dependence of the potentials was not taken into account in this paper. However, LFP data coming from experiments usually have the form of several time series — one for each electrode. Modeling these time series, relationships between them and incorporating this knowledge in the estimation may reveal more information about the examined region.

A possible way of extending the framework described in this paper would be to add time dependence to the basis functions introduced in Section 3. In the simplest case one

could think of basis functions that factorise into the product of two seperate location and time dependent factors:

$$\widetilde{b}_i(\mathbf{x}, t) = \widetilde{b}_{i1}(\mathbf{x})\widetilde{b}_{i2}(t),$$

where $\widetilde{b}_{i2}(t)$ could have a 'step' or a gaussian shape.

If we calculate the potential generated by $\widetilde{b}_i$ in every moment t, we get a set of potential basis functions $b_i(\mathbf{x}, t)$. We are therefore free to construct kernels as in (6) and (16), run the kCSD method and obtain a time dependent CSD estimator.

Direct kCSD method Up till now we have always derived kernels K and $\widetilde{K}$ from the basis functions via equations (6) and (16). One can also try defining kernel K directly, omitting the introduction of basis functions. It is shown in Shawe-Taylor & Christiani (2004) (Theorem 3.11) that as long as a kernel function K is positive definite, then there exists an RKHS $\mathcal{H}$ and an equivalent mapping $\phi : \mathbb{R} \longrightarrow \mathcal{H}$ such that:

$$K(x, y) = \langle \phi(x), \phi(y) \rangle.$$

We are therefore free to model the potentials with kernels typically used in learning algorithms (e.g. a Gaussian kernel), as presented for instance in Schoelkopf & Smola (2002), Chapter 2.3. To model CSD it rests to find the equivalent cross-kernel. This can be done regarding the following equation:

$$K(x, y) = \mathcal{A}_y \widetilde{K}(x, y),$$

where by $\mathcal{A}_y$ we denote operator $\mathcal{A}$ acting on the second variable, so we can write

$$\widetilde{K}(x, y) = [\mathcal{A}_y]^{-1} K(x, y).$$

Calculating $\widetilde{K}$ involves inverting operator $\mathcal{A}_y$ which is simple in the three dimensional case where the inverse operator is just the Laplacian. However, in 1D and 2D cases this operator depends on the model of the tissue in the directions normal to the space spanned by the electrodes, so its inversion is more involved.

Our preliminary numerical experiments with the 3D case indicate that this 'direct kCSD' method, as we call it, is even faster, very easy to calculate, and is very stable. A thorough study is underway.

Beyond over-fitting We have assumed here that the data are precise (measured without errors) which is never the case in practice. If we consider some model of additive noise of measurement we can take it into account by modifying the error funcition (7). Including regularization by applying the SVM algorithm (Vapnik 1998, Schoelkopf & Smola 2002, Shawe-Taylor & Christiani 2004) should reduce the possibility of over-fitting. Also then the problem of inverting $\mathbf{K}$ in (13) would vanish, because the SVM algorithm consists of solving an optimisation problem instead of directly solving a linear system of equations.

Generalized models of tissue conductivity We have assumed in the analysis constant conductivity. This simplifies the problem and in view of the lack of available data on conductivity in many areas, is a natural approach to start. However, as it is now becoming feasible to measure conductivity more and more precisely and as the changing conductivity seems to influence substantially the fields Goto et al. (2010) it is necessary to develop kCSD to incorporate richer models of sources taking into account space-dependent and perhaps non-scalar conductivity. One important example which calls for a dedicated approach is that of slices on multielectrode arrays (MEA).

Connection to source reconstruction from EEG CSD reconstruction is similar in spirit to reconstruction of sources in EEG (He & Lian 2005), however, since extracellular recordings of LFP are taken much closer to the sources than in the case of EEG, one builds different models (see the discussion in Łęski, Pettersen, Tunstall, Einevoll, Gigg & Wójcik (2010)). Despite the difference in physics, we believe that the same statistical setting can be adapted to the case of human electroencephalography helping in source localization there. The difference would be in the basis elements $b_i(x)$, as for EEG one would naturally consider distributions of dipoles. The connection between the sources and potentials would have to take into account the complication of changing conductivity in the skull, skin, etc and would probably be the most challenging problem. Otherwise, the framework presented should apply.

Acknowledgements

This work was supported by the Polish Ministry of Science and Higher Education grant PBZ/MNiSW/07/2006/1 and by the infrastructural grant from the Polish Ministry of Regional Development, POIG.02.03.00-00-003/09.

A Appendix

In this appendix we provide proofs of some mathematical results stated in the paper.

A.1 Proof of Theorem 2.3

Proposition A.1 *Suppose $b_1, ..., b_n : A \subset \mathbb{R}^d \longrightarrow \mathbb{R}$ are piecewise smooth, linearly independent functions. For every $m \leq n$ there exists a set of points $x_1, ..., x_m$, such that the matrix:*

$$\begin{bmatrix} b_1(x_1) & b_1(x_2) & \cdots & b_1(x_m) \\ b_2(x_1) & b_2(x_2) & \cdots & b_2(x_m) \\ \vdots & \vdots & \ddots & \vdots \\ b_m(x_1) & b_m(x_2) & \cdots & b_m(x_m) \end{bmatrix}$$

is invertible.

Proof The proof will be carried out by induction. First, let us prove the proposition for two functions $b_1(x), b_2(x)$. Take x_1 such that $b_2(x_1) \neq 0$. Let $c = \frac{b_1(x_1)}{b_2(x_1)}$ and choose x_2 such that $b_1(x_2) \neq c \cdot b_2(x_2)$. Such a point must exist, otherwise b_1 and b_2 would be linearly dependent. Then the matrix:

$$\begin{bmatrix} b_1(x_1) & b_1(x_2) \\ b_2(x_1) & b_2(x_2) \end{bmatrix} \tag{38}$$

is invertible.

Now let $m \leq n$ and suppose that there exist such points $x_1, ..., x_{m-1}$, that the matrix:

$$\begin{bmatrix} b_1(x_1) & b_1(x_2) & \cdots & b_1(x_{m-1}) \\ b_2(x_1) & b_2(x_2) & \cdots & b_2(x_{m-1}) \\ \vdots & \vdots & \ddots & \vdots \\ b_{m-1}(x_1) & b_{m-1}(x_2) & \cdots & b_{m-1}(x_{m-1}) \end{bmatrix} \tag{39}$$

is invertible. Let $r_1, ..., r_{m-1}$ denote the rows of matrix (39).

Extend matrix (39) in the following manner:

$$\begin{bmatrix} b_1(x_1) & b_1(x_2) & \cdots & b_1(x_{m-1}) \\ b_2(x_1) & b_2(x_2) & \cdots & b_2(x_{m-1}) \\ \vdots & \vdots & \ddots & \vdots \\ b_{m-1}(x_1) & b_{m-1}(x_2) & \cdots & b_{m-1}(x_{m-1}) \\ b_m(x_1) & b_m(x_2) & \cdots & b_m(x_{m-1}) \end{bmatrix}. \tag{40}$$

If we denote the m-th row of matrix (40) by r_m, there exists a unique set of real numbers $a_1, ..., a_{m-1}$ such that

$$a_1 r_1 + a_2 r_2 + ... + a_{m-1} r_{m-1} = r_m.$$

Then, there exists a point x_m such that

$$a_1 b_1(x_m) + a_2 b_2(x_m) + ... + a_{m-1} b_{m-1}(x_m) \neq b_m(x_m).$$

otherwise b_m would be a linear combination of $b_1, ..., b_{m-1}$. Therefore, matrix

$$\begin{bmatrix} b_1(x_1) & b_1(x_2) & \cdots & b_1(x_{m-1}) & b_1(x_m) \\ b_2(x_1) & b_2(x_2) & \cdots & b_2(x_{m-1}) & b_2(x_m) \\ \vdots & \vdots & \ddots & \vdots & \vdots \\ b_{m-1}(x_1) & b_{m-1}(x_2) & \cdots & b_{m-1}(x_{m-1}) & b_{m-1}(x_m) \\ b_m(x_1) & b_m(x_2) & \cdots & b_m(x_{m-1}) & b_m(x_m) \end{bmatrix}, \tag{41}$$

has linearly independent rows and so is invertible.

□

Proof of the theorem

(i) It is immediately seen that:

$$f(x) = \sum_{j=1}^{l} \alpha_j \sum_{i=1}^{n} b_i(x_j) b_i(x) = \sum_{i=1}^{n} \left(\sum_{j=1}^{l} \alpha_j b_i(x_j) \right) b_i(x) = \sum_{i=1}^{n} a_i b_i(x).$$

(ii) Assuming $f(x) = a_1 b_1(x) + ... + a_n b_n(x)$ we want to prove the existence of such $x_1, ..., x_n$ and $\alpha_1, ..., \alpha_n$, that

$$f(x) = \sum_{i=1}^{n} \alpha_i K(x_i, x). \tag{42}$$

If we rewrite equation (42) directly we get:

$$\begin{aligned} f(x) &= \alpha_1 \left[b_1(x_1) b_1(x) + b_2(x_1) b_2(x) + ... + b_n(x_1) b_n(x) \right] \\ &+ \alpha_2 \left[b_1(x_2) b_1(x) + b_2(x_2) b_2(x) + ... + b_n(x_2) b_n(x) \right] \\ &... \\ &+ \alpha_n \left[b_1(x_n) b_1(x) + b_2(x_n) b_2(x) + ... + b_n(x_n) b_n(x) \right]. \end{aligned}$$

Expressing our task using matrix notation: we are looking for such $x_1, ..., x_n, \alpha_1, ..., \alpha_n$, that:

$$\begin{bmatrix} b_1(x) \\ \vdots \\ b_n(x) \end{bmatrix}^T \begin{bmatrix} b_1(x_1) & ... & b_1(x_n) \\ \vdots & \ddots & \vdots \\ b_n(x_1) & ... & b_n(x_n) \end{bmatrix} \begin{bmatrix} \alpha_1 \\ \vdots \\ \alpha_n \end{bmatrix} = \begin{bmatrix} b_1(x) \\ \vdots \\ b_n(x) \end{bmatrix}^T \begin{bmatrix} a_1 \\ \vdots \\ a_n \end{bmatrix} \tag{43}$$

or shortly:

$$\mathbf{b}(x)^T \mathbf{B}(x_1, ..., x_n)\, \alpha = \mathbf{b}(x)^T \mathbf{a}.$$

From Proposition A.1 it follows, that there exist such points $x_1, ..., x_n$, that matrix $\mathbf{B}(x_1, ..., x_n)$ is invertible. Taking $\alpha_1, ..., \alpha_n$ as

$$\alpha = [\mathbf{B}(x_1, ..., x_n)]^{-1} \mathbf{a}$$

completes construction.

(iii) Take $f(x) = \sum_{i=1}^{n} a_i b_i(x)$ with $a_i = \sum_{j=1}^{l} \alpha_j b_i(x_j)$ (see *(i)* above). Then

$$\begin{aligned} \|f\|_{\mathcal{F}}^2 = \sum_{i=1}^{n} a_i^2 &= \sum_{i=1}^{n} \left(\sum_{j=1}^{l} \alpha_j b_i(x_j) \right) \left(\sum_{k=1}^{l} \alpha_k b_i(x_k) \right) \\ &= \sum_{i=1}^{n} \sum_{j=1}^{l} \sum_{k=1}^{l} \alpha_j \alpha_k b_i(x_j) b_i(x_k) \\ &= \sum_{j=1}^{l} \sum_{k=1}^{l} \alpha_j \alpha_k K(x_j, x_k) \\ &= \|f\|_{\mathcal{H}}^2 \end{aligned}$$

□

A.2 Proof of Theorem 2.4

Proposition A.2 *Let* $\mathcal{S} = span\,\{K(x_1, \cdot), ..., K(x_n, \cdot)\}$ *and* $f \in \mathcal{H}$. *Then*

$$f \perp S \Leftrightarrow \forall_i f(\mathbf{x}_i) = 0$$

Proof

Suppose that $f \perp S$ that is $f \perp K(x_i, \cdot)$ for all i. Considering the reproducing property this means, that for all i:

$$(f, K(x_i, \cdot)) = f(x_i) = 0. \tag{44}$$

On the other hand, the reproducing property implies that if $\forall_i f(x_i) = 0$ then $f \perp \mathcal{S}$.

□

Proof of the Theorem

Let $\mathcal{S}$ be defined as in Proposition A.2. One can decompose space $\mathcal{H}$:

$$\mathcal{H} = \mathcal{S} \oplus \mathcal{S}^{\perp}. \tag{45}$$

Now each function $f \in \mathcal{H}$ can also be decomposed:

$$f = f_{\mathcal{S}} + f^{\perp}, \tag{46}$$

so that $f_{\mathcal{S}} \in \mathcal{S}$, $f^{\perp} \in \mathcal{S}^{\perp}$. Take

$$f^* \in \arg\min_{f \in \mathcal{H}} \sum_{i=1}^{k} \left(f(\mathbf{x}_i) - f_i\right)^2.$$

From Proposition A.2 we see that for all i:

$$f^*(\mathbf{x}_i) = f^*_{\mathcal{S}}(\mathbf{x}_i) \Rightarrow (f^*(\mathbf{x}_i) - f_i)^2 = (f^*_{\mathcal{S}}(\mathbf{x}_i) - f_i)^2, \tag{47}$$

which implies that also $f^*_{\mathcal{S}} \in \mathcal{M}$. Now, minimum of err is 0 which can be achieved if and only if $\forall i : f^*_{\mathcal{S}}(\mathbf{x}_i) - f_i = 0$, that is

$$f_i = \sum_j \beta_j K(x_j, x_i).$$

Since we assumed that matrix

$$\begin{bmatrix} K(x_1,x_1) & \dots & K(x_1,x_k) \\ \vdots & \ddots & \vdots \\ K(x_k,x_1) & \dots & K(x_k,x_k) \end{bmatrix}$$

is invertible, we can take

$$\begin{bmatrix} \beta_1 \\ \vdots \\ \beta_k \end{bmatrix} = \begin{bmatrix} K(x_1,x_1) & \dots & K(x_1,x_k) \\ \vdots & \ddots & \vdots \\ K(x_k,x_1) & \dots & K(x_k,x_k) \end{bmatrix}^{-1} \begin{bmatrix} f_1 \\ \vdots \\ f_k \end{bmatrix}.$$

Then the function

$$f^*_{\mathcal{S}}(x) = \sum_{i=1}^{k} \beta_i K(x_i, x)$$

is a unique minimizer in $\mathcal{S}$. Therefore, for all $f^* \in \mathcal{M}$ we have:

$$f^* = f^*_{\mathcal{S}} + f^{*\perp}. \tag{48}$$

If we calculate the norm of f^* in (48) we get:

$$\|f^*\|^2 = \langle f^*_{\mathcal{S}} + f^{*\perp}, f^*_{\mathcal{S}} + f^{*\perp} \rangle = \|f^*_{\mathcal{S}}\|^2 + \|f^{*\perp}\|.$$

It is therefore clear that $f^*_{\mathcal{S}}$ has the smallest norm in $\mathcal{M}$.

□

B Specification of the sources used in the tests

In this appendix we provide detailed information about the sources used in testing kCSD method in Section 4.

B.1 'Large sources'

The 'large sources' were generated using the following MATLAB function:

```
function f = test_csd(x,y,z)

zz = [0.4; -0.3; -0.1; 0.6];
zs = [0.2; 0.3; 0.4; 0.2];

f1 = 0.5965*exp((-(x-0.1350).^2 - (y-0.8628)^2)/0.4464)*...
 exp(-(z-zz(1))^2/zs(1))/exp(-(zz(1))^2/zs(1));
f2 = -0.9269*exp((-2*(x-0.1848).^2 - (y-0.0897)^2)/0.2046)*...
 exp(-(z-zz(2))^2/zs(2))/exp(-(zz(2))^2/zs(2));
f3 = 0.5910*exp((-3*(x-1.3189).^2 - (y-0.3522)^2)/0.2129)*...
 exp(-(z-zz(3))^2/zs(3))/exp(-(zz(3))^2/zs(3));
f4 = -0.1963*exp((-4*(x-1.3386).^2 - (y-0.5297)^2)/0.2507)*...
 exp(-(z-zz(4))^2/zs(4))/exp(-(zz(4))^2/zs(4));

f= f1+f2+f3+f4;
```

Note that the sources used in this paper have product structure which means that the above function was evaluated only for $z = 0$ and we assumed a step profile in z variable. More general sources were considered in Łęski, Pettersen, Tunstall, Einevoll, Gigg & Wójcik (2010).

B.2 'Small sources'

Let a, μ_1, μ_2 and $\mathbf{C}$ be the parameters (amplitude, mean, covariance matrix) of the following Gaussian function:

$$G_{a,\mu_1,\mu_2,\mathbf{C}}(x,y) = \frac{a}{2\pi\sqrt{\det \mathbf{C}}} \exp\left[-\frac{1}{2}\begin{pmatrix} x-\mu_1 \\ y-\mu_2 \end{pmatrix}^{\mathbf{T}} \mathbf{C}^{-1} \begin{pmatrix} x-\mu_1 \\ y-\mu_2 \end{pmatrix}\right].$$

The 'small sources' dataset was generated by a sum of four such Gaussians with parameters given in the table below:

Number	a	μ_1	μ_2	$\mathbf{C}$
1	0.2	0.2	0.3	$\begin{pmatrix} 0.002 & 0 \\ 0 & 0.008 \end{pmatrix}$
2	−0.25	0.2	0.6	$\begin{pmatrix} 0.005 & 0 \\ 0 & 0.01 \end{pmatrix}$
3	0.24	0.5	0.3	$\begin{pmatrix} 0.0024 & 0 \\ 0 & 0.008 \end{pmatrix}$
4	−0.2	0.5	0.6	$\begin{pmatrix} 0.005 & 0 \\ 0 & 0.01 \end{pmatrix}$

B.3 Random Gaussian sources

The random Gaussian sources were constructed according to the following algorithm (all probability distributions are uniform):

1. choose randomly $r_{\min}$ between 0.1 and 0.2, let $r_{\max} = 2r_{\min}$,
2. choose number n of Gaussian sources, $4 \leq n \leq 8$,
3. for each source choose amplitude a between -1 and 1, angle ϑ between 0 and 2π, position of the source (x_0, y_0) in the square $[0, 1.4]^2$, and σ_x, σ_y between $r_{\min}$ and $r_{\max}$,
4. the test CSD distribution is equal to the sum of n terms, each of the form

$$G(x, y) = a \exp\left[-\mathbf{x}^{\mathbf{T}}\mathbf{A}\mathbf{x}\right],$$

where $\mathbf{x} = \begin{pmatrix} x - x_0 \\ y - y_0 \end{pmatrix}$, and $\mathbf{A} = \begin{pmatrix} \frac{\cos^2\vartheta}{2\sigma_x^2} + \frac{\sin^2\vartheta}{2\sigma_y^2} & -\frac{\sin 2\vartheta}{4\sigma_x^2} + \frac{\sin 2\vartheta}{4\sigma_y^2} \\ -\frac{\sin 2\vartheta}{4\sigma_x^2} + \frac{\sin 2\vartheta}{4\sigma_y^2} & \frac{\sin^2\vartheta}{2\sigma_x^2} + \frac{\cos^2\vartheta}{2\sigma_y^2} \end{pmatrix}$.

(see http://en.wikipedia.org/wiki/Gaussian_function).

B.4 1-D sources

The one-dimensional sources were constructed in the following manner as a mixture of two Gaussians:

$$G_{A_1,\mu_1,\sigma_1,A_2,\mu_2,\sigma_2} = A_1 \exp\left(-\frac{(x-\mu_1)^2}{2\pi\sigma_1}\right) + A_2 \exp\left(-\frac{(x-\mu_2)^2}{2\pi\sigma_2}\right).$$

The parameter values were:

A_1	μ_1	σ_1	A_2	μ_2	σ_2
1	2	0.5	0.5	7	1

References

Aronszajn, N. (1950), 'Theory of reproducing kernels', *Transactions of the American Mathematical Society* **68**(3), 337–404.

Bakker, R., Schubert, D., Levels, K., Bezgin, G., Bojak, I. & Kötter, R. (2009), 'Classification of cortical microcircuits based on micro-electrode-array data from slices of rat barrel cortex.', *Neural Netw* **22**(8), 1159–1168.

Barthó, P., Hirase, H., Monconduit, L., Zugaro, M., Harris, K. D. & Buzsáki, G. (2004), 'Characterization of neocortical principal cells and interneurons by network interactions and extracellular features.', *J Neurophysiol* **92**(1), 600–608.

Berens, P., Keliris, G. A., Ecker, A. S., Logothetis, N. K. & Tolias, A. S. (2008), 'Feature selectivity of the gamma-band of the local field potential in primate primary visual cortex', *Frontiers in Neuroscience* **2**(2), 199–207.

Buzsáki, G. (2004), 'Large-scale recording of neuronal ensembles.', *Nat Neurosci* **7**(5), 446–451.

Charvet, G., Rousseau, L., Billoint, O., Gharbi, S., Rostaing, J.-p., Trevisiol, M., Bourgerette, A., Chauvet, P., Mercier, B., Colin, M., Spirkovitch, S., Meyrand, P. & Yvert, B. (2010), 'BioMEA: A versatile high-density 3D microelectrode array system using integrated electronics', *Biosensors and Bioelectronics* **25**, 1889–1896.

Csicsvari, J., Henze, D. A., Jamieson, B., Harris, K. D., Sirota, A., Barthó, P., Wise, K. D. & Buzsáki, G. (2003), 'Massively parallel recording of unit and local field potentials with silicon-based electrodes.', *J Neurophysiol* **90**(2), 1314–1323.

de Solages, C., Szapiro, G., Brunel, N., Hakim, V., Isope, P., Buisseret, P., Rousseau, C., Barbour, B. & Léna, C. (2008), 'High-frequency organization and synchrony of activity in the purkinje cell layer of the cerebellum.', *Neuron* **58**(5), 775–788.

Einevoll, G. T., Pettersen, K. H., Devor, A., Ulbert, I., Halgren, E. & Dale, A. M. (2007), 'Laminar population analysis: estimating firing rates and evoked synaptic activity from multielectrode recordings in rat barrel cortex.', *J Neurophysiol* **97**(3), 2174–2190.

Freeman, J. A. & Nicholson, C. (1975), 'Experimental optimization of current source-density technique for anuran cerebellum.', *J Neurophysiol* **38**(2), 369–382.

Frey, U., Egert, U., Heer, F., Hafizovic, S. & Hierlemann, A. (2009), 'Microelectronic system for high-resolution mapping of extracellular electric fields applied to brain slices', *Biosensors and Bioelectronics* **24**, 2191–2198.

Goto, T., Hatanaka, R., Ogawa, T., Sumiyoshi, A., Riera, J. J. & Kawashima, R. (2010), 'An evaluation of the conductivity profile in the somatosensory barrel cortex of wistar rats.', *J Neurophysiol* .

Haberly, L. B. & Shepherd, G. M. (1973), 'Current-density analysis of summed evoked potentials in opossum prepyriform cortex.', *J Neurophysiol* **36**(4), 789–802.

He, B. & Lian, J. (2005), Electrophysiological neuroimaging, *in* B. He, ed., 'Neural Engineering', Kluwer Academic, New York.

Hunt, M. J., Falinska, M., Leski, S., Wójcik, D. K. & Kasicki, S. (2010), 'Differential effects produced by ketamine on oscillatory activity recorded in the rat hippocampus, dorsal striatum and nucleus accumbens.', *J Psychopharmacol* .

Imfeld, K., Neukom, S., Maccione, A., Bornat, Y., Martinoia, S., Farine, P.-A., Koudelka-hep, M. & Berdondini, L. (2008), 'Large-Scale, High-Resolution Data Acquisition System for Extracellular Recording of Electrophysiological Activity', *IEEE TRANSACTIONS ON BIOMEDICAL ENGINEERING* **55**(8), 2064–2073.

Katzner, S., Nauhaus, I., Benucci, A., Bonin, V., Ringach, D. L. & Carandini, M. (2009), 'Local Origin of Field Potentials in Visual Cortex', *Neuron* **61**(1), 35–41.

Kreiman, G., Hung, C. P., Kraskov, A., Quiroga, R. Q., Poggio, T. & Dicarlo, J. J. (2006), 'Object Selectivity of Local Field Potentials and Spikes in the Macaque Inferior Temporal Cortex', *Neuron* **49**, 433–445.

Lakatos, P., Shah, A. S., Knuth, K. H., Ulbert, I., Karmos, G. & Schroeder, C. E. (2005), 'An Oscillatory Hierarchy Controlling Neuronal Excitability and Stimulus Processing in the Auditory Cortex', *Journal of Neurophysiology* **94**, 1904–1911.

Lindén, H., Pettersen, K. H. & Einevoll, G. T. (2010), 'Intrinsic dendritic filtering gives low-pass power spectra of local field potentials', *Journal of Computational Neuroscience*

Lipton, M. L., Fu, K.-M. G., Branch, C. A. & Schroeder, C. E. (2006), 'Ipsilateral hand input to area 3b revealed by converging hemodynamic and electrophysiological analyses in macaque monkeys', *Journal of Neuroscience* **26**, 180–185.

Liu, J. & Newsome, W. T. (2006), 'Local Field Potential in Cortical Area MT: Stimulus Tuning and Behavioral Correlations', *Journal of Neuroscience* **26**(30), 7779 –7790.

Lorente de No, R. (1947), 'A study of nerve physiology.', *Studies from the Rockefeller Institute for Medical Research* **131**, 1–496.

Łęski, S., Kublik, E., Świejkowski, D. A., Wróbel, A. & Wójcik, D. K. (2010), 'Extracting functional components of neural dynamics with independent component analysis and inverse current source density', *Journal of Computational Neuroscience* .

Łęski, S., Pettersen, K. H., Tunstall, B., Einevoll, G., Gigg, J. & Wójcik, D. K. (2010), Inverse current source density method in two dimensions: Inferring neural activation from multielectrode recordings. Neuroinformatics.
ęski et al.

Łęski, S., Wójcik, D. K., Tereszczuk, J., Świejkowski, D. A., Kublik, E. & Wróbel, A. (2007), 'Inverse current-source density method in 3d: reconstruction fidelity, boundary effects, and influence of distant sources.', *Neuroinformatics* **5**(4), 207–222.

Mitzdorf, U. (1985), 'Current source-density method and application in cat cerebral cortex: investigation of evoked potentials and eeg phenomena.', *Physiol Rev* **65**(1), 37–100.

Nicholson, C. & Freeman, J. A. (1975), 'Theory of current source-density analysis and determination of conductivity tensor for anuran cerebellum.', *J Neurophysiol* **38**(2), 356–368.

Normann, R. A., Maynard, E. M., Rousche, P. J. & Warren, D. J. (1999), 'A neural interface for a cortical vision prosthesis.', *Vision Res* **39**(15), 2577–2587.

Nunez, P. L. & Srinivasan, R. (2005), *Electric Fields of the Brain: The Neurophysics of EEG*, Oxford University Press.

Pettersen, K. H., Devor, A., Ulbert, I., Dale, A. M. & Einevoll, G. T. (2006), 'Current-source density estimation based on inversion of electrostatic forward solution: effects of finite extent of neuronal activity and conductivity discontinuities.', *J Neurosci Methods* **154**(1-2), 116–133.

Pettersen, K. H., Hagen, E. & Einevoll, G. T. (2008), 'Estimation of population firing rates and current source densities from laminar electrode recordings.', *J Comput Neurosci* **24**(3), 291–313.
URL: *http://dx.doi.org/10.1007/s10827-007-0056-4*

Pitts, W. H. (1952), Investigations on synaptic transmission, *in* 'Cybernetics, Trans. 9th Conf. Josiah Macy Foundation H. von Foerster', New York, pp. 159–166.

Plonsey, R. (1969), *Bioelectric phenomena*, McGraw-Hill Book Company, New York.

Rajkai, C., Lakatos, P., Chen, C.-M., Pincze, Z., Karmos, G. & Schroeder, C. E. (2008), 'Transient cortical excitation at the onset of visual fixation', *Cerebral Cortex* **18**, 200–209.

Schoelkopf, B. & Smola, A. (2002), *Learning with Kernels*, Massachusets Institute of Technology.

Schroeder, C. E., Tenke, C. E. & Givre, S. J. (1992), 'Subcortical contributions to the surface-recorded flash-vep in the awake macaque', *Electroencephalography and Clinical Neurophysiology* **84**, 219–231.

Shawe-Taylor, J. & Christiani, N. (2004), *Kernel Methods for Pattern Analysis*, Cambridge University Press.

Sher, A., Chichilnisky, E., Dabrowski, W., Grillo, A., Grivich, M., Gunning, D., Hottowy, P., Kachiguine, S., Litke, A., Mathieson, K. & Petrusca, D. (2007), 'Large-scale multielectrode recording and stimulation of neural activity', *Nuclear Instruments and Methods in Physics Research A* **579**, 895–900.

Shi, T., Belkin, M. & Yu, B. (2008), Data spectroscopy: Learning mixture models using eigenspaces of convolution operators, *in* 'Proceedings of the 25-th International Conference on Machine Learning', Helsinki, Finland.

Vapnik, V. N. (1998), *Statistical Learning Theory*, John Wiley & Sons.

Ward, M. P., Rajdev, P., Ellison, C. & Irazoqui, P. P. (2009), 'Toward a comparison of microelectrodes for acute and chronic recordings', *Brain Research* **1282**, 183–200.

Wirth, C. & Lüscher, H.-R. (2004), 'Spatiotemporal evolution of excitation and inhibition in the rat barrel cortex investigated with multielectrode arrays.', *J Neurophysiol* **91**(4), 1635–1647.

Wójcik, D. K. & Łęski, S. (2010), 'Current source density reconstruction from incomplete data', *Neural Computation* **22**, 48–60.

Xing, D., Yeh, C.-I. & Shapley, R. M. (2009), 'Spatial Spread of the Local Field Potential and its Laminar Variation in Visual Cortex', *Journal of Neuroscience* **29**(37), 11540 –11549.

Ylinen, A., Bragin, A., Nadasdy, Z., Jando, G., Szabo, I., Sik, A. & Buzsaki, G. (1995), 'Sharp Wave-Associated High-Frequency Oscillation (200 Hz) in the Intact Hippocampus: Network and Intracellular Mechanisms', *Journal of Neuroscience* **15**(January), 30–46.